

Superchiral fields generated by nanostructures and their applications for chiral sensing

Huizhen Zhang(张慧珍), Weixuan Zhang(张蔚暄), Saisai Hou(侯赛赛), Rongyao Wang(王荣瑶), and Xiangdong Zhang(张向东)

Citation: Chin. Phys. B, 2021, 30 (**11**): 113303. DOI: 10.1088/1674-1056/ac11df
Journal homepage: http://cpb.iphy.ac.cn; http://iopscience.iop.org/cpb

What follows is a list of articles you may be interested in

Collective excitations and quantum size effects on the surfaces of Pb(111) films: An experimental study

Yade Wang(王亚德), Zijian Lin(林子荐), Siwei Xue(薛思玮), Jiade Li(李佳德), Yi Li(李毅), Xuetao Zhu(朱学涛), and Jiandong Guo(郭建东)

Chin. Phys. B, 2021, 30 (**7**): 077308. DOI: 10.1088/1674-1056/abfbcd

Quantifying plasmon resonance and interband transition contributions in photocatalysis of gold nanoparticle

Liang Dong(董亮), Chengyun Zhang(张成云), Lei Yan(严蕾), Baobao Zhang(张宝宝), Huan Chen(陈环), Xiaohu Mi(弥小虎), Zhengkun Fu(付正坤), Zhenglong Zhang(张正龙), and Hairong Zheng(郑海荣)

Chin. Phys. B, 2021, 30 (**7**): 077301. DOI: 10.1088/1674-1056/abfa0c

High sensitive chiral molecule detector based on the amplified lateral shift in Kretschmann configuration involving chiral TDBCs

Song Wang(王松), Qihui Ye(叶起惠), Xudong Chen(陈绪栋), Yanzhu Hu(胡燕祝), and Gang Song(宋钢)

Chin. Phys. B, 2021, 30 (**6**): 067301. DOI: 10.1088/1674-1056/abdda6

Quantization of the band at the surface of charge density wave material 2H-$TaSe_2$

Man Li(李满), Nan Xu(徐楠), Jianfeng Zhang(张建丰), Rui Lou(娄睿), Ming Shi(史明), Lijun Li(黎丽君), Hechang Lei(雷和畅), Cedomir Petrovic, Zhonghao Liu(刘中灏), Kai Liu(刘凯), Yaobo Huang(黄耀波), and Shancai Wang(王善才)

Chin. Phys. B, 2021, 30 (**4**): 047305. DOI: 10.1088/1674-1056/abe9a8

Chiral asymmetry of anti-symmetric coordinates studied by the Raman differential bond polarizability of *S*-phenylethylamine

Shen Hong-Xia, Wu Guo-Zhen, Wang Pei-Jie

Chin. Phys. B, 2012, 21 (**12**): 123301. DOI: 10.1088/1674-1056/21/12/123301

TOPICAL REVIEW — Optical field manipulation

Superchiral fields generated by nanostructures and their applications for chiral sensing*

Huizhen Zhang(张慧珍), Weixuan Zhang(张蔚暄), Saisai Hou(侯赛赛), Rongyao Wang(王荣瑶), and Xiangdong Zhang(张向东)†

Key Laboratory of Advanced Optoelectronic Quantum Architecture and Measurements of Ministry of Education, Beijing Key Laboratory of Nanophotonics & Ultrafine Optoelectronic Systems, School of Physics, Beijing Institute of Technology, Beijing 100081, *China*

(Received 18 April 2021; revised manuscript received 29 June 2021; accepted manuscript online 7 July 2021)

Chirality is ubiquitous in natural world. Although with similar physical and chemical properties, chiral enantiomers could play different roles in biochemical processes. Discrimination of chiral enantiomers is extremely important in biochemical, analytical chemistry, and pharmaceutical industries. Conventional chiroptical spectroscopic methods are disadvantageous at a limited detection sensitivity because of the weak signals of natural chiral molecules. Recently, superchiral fields were proposed to effectively enhance the interaction between light and molecules, allowing for ultrasensitive chiral detection. Intensive theoretical and experimental works have been devoted to generation of superchiral fields based on artificial nanostructures and their application in ultrasensitive chiral sensing. In this review, we present a survey on these works. We begin with the introduction of chiral properties of electromagnetic fields. Then, the optical chirality enhancement and ultrasensitive chiral detection based on chiral and achiral nanostructures are discussed respectively. Finally, we give a short summary and a perspective for the future ultrasensitive chiral sensing.

Keywords: superchiral fields, chiral detection, chiral nanostructures, achiral nanostructures

PACS: 33.55.+b, 73.20.Mf, 81.05.Xj, 78.67.Bf **DOI:** 10.1088/1674-1056/ac11df

1. Introduction

An object that cannot be superimposed onto its mirror image is called chiral.[1] Chirality is ubiquitous throughout the universe and can be observed at widely different scales, from the shape of galaxies down to sub-atomic particles. The two separate entities within a chiral pair are referred to as left-handed and right-handed structures, or for concision, as "enantiomers". Enantiomers show similar physical and chemical properties because of their identical functional groups and compositions, however, they could play different roles in biochemical processes. Discrimination of these chiral enantiomers is indeed critically important in aspects of biochemistry, analytical chemistry, drug development, and so on.[2,3] The conventional chiroptical techniques for enantiomers discrimination are to detect the interactions between chiral molecules and circular polarized lights.[4] The most widely used chiroptical spectroscopic techniques are circular dichroism (CD),[5] vibrational circular dichroism (VCD),[6] optical rotation dispersion (ORD),[7] and Raman optical activity (ROA),[8,9] *etc*. CD and VCD describe the different absorption of left-handed circularly polarized (LCP) light and right-handed circularly polarized (RCP) incident light for chiral samples. CD measures this different absorption in the ultraviolet and visible spectrum, while VCD extends this measurement to the infrared spectrum. ORD describes the polarization rotation of a linearly polarized incident light passing through chiral materials. ROA observes the difference in Raman scattering from chiral molecules for LCP and RCP incident light, or a small circularly polarized component in the scattered light.[10–12]

There are limitations for conventional chiroptical spectroscopic methods. The chiral arrangement of molecular bonds is much smaller than the helical pitch of circularly polarized light (CPL), which makes the chiral molecules hardly "perceive" the chiral structure of the circularly polarized field. Thus, chiroptical effects of natural chiral molecules are very weak. This extreme weakness of chiroptical signals makes it difficult to obtain structural information with high precision in conventional chiroptical spectroscopic methods, and forces the use of large volumes or high concentration samples for bulk measurement.

An effective method to solve this problem is to enhance optical chirality of electromagnetic fields, which determines the strength of interaction between electromagnetic fields and chiral molecules. Early works proposed by Tang and Cohen[13,14] have shown that superchiral fields, which possess larger optical chirality than circular polarized light (CPL), can significantly enhance molecular chiroptical effects, allowing for ultrasensitive detection of chiral molecules. Remarkably, the superchiral field not only leads to significant enhancement

*Project supported by the National Natural Science Foundation of China (Grant Nos. 91850205 and 11904021).

†Corresponding author. E-mail: zhangxd@bit.edu.cn

© 2021 Chinese Physical Society and IOP Publishing Ltd

for CD signals, it triggers development of almost all the chiroptical spectroscopy technologies, including VCD, ORD, and ROA. Because of its high importance in all these applications, the superchiral field has bloomed in the last ten years, and intense theoretical and experimental studies have been devoted to the generation of superchiral near fields and their application in ultrasensitive chiral sensing with the help of artificial nanostructures. Herein we review these works on generation of superchiral fields and the corresponding ultrasensitive chirality sensing. The optical chirality of electromagnetic field is introduced in Section 2. Then the enhancement of optical chirality and chiral detection based on chiral and achiral nanostructures is discussed in Sections 3 and 4, respectively. Finally, we give a short summary and a perspective of the future ultrasensitive chiral molecular sensing.

2. The study on chiral properties of electromagnetic fields

In addition to using amplitude, polarization and phase to describe the characteristics of light field, the optical chirality C has also been introduced to describe the chiral properties of light field. The optical chirality is expressed as[14–16]

$$C = \frac{\varepsilon_0}{2}\boldsymbol{E}\cdot(\nabla\times\boldsymbol{E}) + \frac{1}{2\mu_0}\boldsymbol{B}\cdot(\nabla\times\boldsymbol{B}), \tag{1}$$

where ε_0 and μ_0 correspond to permittivity and permeability of free space respectively, $\boldsymbol{E}$ and $\boldsymbol{B}$ are the local electric and magnetic fields.[15]

This physical quantity is defined originally by Lipkin in 1964, but it did not have a physical meaning. It was not until 2010 that Tang and Cohen pointed out that the optical chirality determines the asymmetry in the rates of excitation between a small chiral molecule and counterpart, such a concept has attracted great attention. The good correspondence between superchiral fields and CD signals has been demonstrated. A chiral molecule subjected to a monochromatic electromagnetic field generates an electric dipole moment $\boldsymbol{p}$ and a magnetic dipole moment $\boldsymbol{m}$ given by[13,17,18]

$$\boldsymbol{p} = \alpha\boldsymbol{E} - \mathrm{i}G\boldsymbol{B}, \quad \boldsymbol{m} = \chi\boldsymbol{B} + \mathrm{i}G\boldsymbol{E}. \tag{2}$$

Here $\alpha = \alpha' + \mathrm{i}\alpha''$, $G = G' + \mathrm{i}G''$ and $\chi = \chi' + \mathrm{i}\chi''$ are complex. α is the electric polarizability, G the isotropic mixed electric-magnetic dipole polarizability and χ the magnetic susceptibility. The absorption rate of the chiral molecule for the left- and right-handed polarized light, $Q_\pm$, can be rewritten according to Ref. [19] in the following form:

$$Q_\pm = \langle\boldsymbol{E}\cdot\boldsymbol{p} + \boldsymbol{B}\cdot\boldsymbol{m}\rangle = \frac{\omega}{2}\mathrm{Im}(\boldsymbol{E}^*\cdot\boldsymbol{p} + \boldsymbol{B}\cdot\boldsymbol{m}), \tag{3}$$

where the brackets indicate an average over time. Expanding the absorption rate using Eq. (2) we have

$$Q_\pm = \frac{\omega}{2}\left(\alpha''|\boldsymbol{E}|^2 + \chi''|\boldsymbol{B}|^2\right) \pm G''\,\mathrm{Im}\,(\boldsymbol{E}^*\cdot\boldsymbol{B}). \tag{4}$$

From Maxwell equation, $C = -(\varepsilon_0/2)[\boldsymbol{E}\cdot\boldsymbol{B}' - \boldsymbol{B}\cdot\boldsymbol{E}']$ and applying the identity $\omega\,\mathrm{Im}\,(\boldsymbol{E}^*\cdot\boldsymbol{B}) = \boldsymbol{E}\cdot\boldsymbol{B}' - \boldsymbol{B}\cdot\boldsymbol{E}'$, we have

$$C = -\frac{\omega_0\varepsilon_0}{2}\,\mathrm{Im}\,[\boldsymbol{E}^*\cdot\boldsymbol{B}]. \tag{5}$$

That is

$$Q_\pm = \frac{2}{\varepsilon_0}\left(\omega U_\mathrm{e}\alpha'' - C^\pm G''\right), \tag{6}$$

where $U_\mathrm{e} = (\varepsilon_0/4)|\boldsymbol{E}|^2$ is the time-average electric energy density, C^+ and C^- represent the superchiral fields excited by the left- and right-handed polarized light, respectively. If we define $\Delta\hat{C} = (C^+ - C^-)/C_\mathrm{CPL}$, C_CPL corresponds to the superchiral field of circularly polarized light, then,

$$CD \propto Q_+ - Q_- = -\frac{2}{\varepsilon_0}G''\left(C^+ - C^-\right) \propto \Delta\hat{C}. \tag{7}$$

This means that the CD is directly proportional to $\Delta\hat{C}$. The detection sensitivity of molecular chiral signals can be greatly enhanced by reasonably designing nanostructures and constructing strong superchiral fields.

3. Superchiral fields generated by chiral nanostructures and their applications for chiral sensing

Chiral nanostructures, whose great chiroptical effects are several orders of magnitude higher than common biomolecules, have attracted great interests in recent years. Despite of such huge CD and ORD signals, chiral nanostructures can also be optically excited to generate superchiral fields, which provides an effective method to detect chiral molecules with a high sensitivity.

3.1. Superchiral fields generated by chiral nanostructures

3.1.1. Chiral nanoclusters

Local electromagnetic fields with enhanced optical chirality arise from enhanced $\boldsymbol{E}$ and $\boldsymbol{B}$ which are parallel and phase shifted with each other, as stated by Eq. (5). Arranging metal nanoparticles into chiral assembles can meet above conditions rather simply and effectively. When illuminated by light with proper energy and momentum, localized surface plasmons (LSPs) can be excited to enhance electromagnetic fields nearby metal nanoparticles. The magnetic field of one nanoparticle can be parallel to electric fields of other particles because of the chiral arrangement. Thus, the chiral near field will be enhanced. Figure 1(a1) displays this optical chirality enhancement in gaps of quasi three-dimensional chiral tetramers.[20] The tetramers are composed of closely spaced silver/gold nanodisks of different heights arranged in chiral. At favorable positions and wavelengths, the optical chirality enhancement factor (C/C_CPL) can even reach 200–300. However, the enhanced optical chirality of these tetramers is not uniform, with rapid sign changes around the gap region, as

shown in Fig. 1(a2), thus the volume-integrated enhancement factor reduced down to the value of about 5.

Nair *et al.* investigated the influence of interparticle distance on optical chirality in chiral plasmonic nanoclusters.[21] Figures 1(b1) and 1(b2) show differential optical chirality enhancement $(C = (C_{\mathrm{LCP}} - C_{\mathrm{PCP}})/C_{\mathrm{CPL}})$ for nanoparticles arranged in helix axis with different aspect ratio r/a (r is the distance between nanoparticles, a is the radius of nanoparticles). Similar to tetramers, the differential optical chirality enhancement is largest in the gap of nanoparticles, and falls off to zero rapidly away from the gap (Fig. (b1)). The relationship between differential optical chirality enhancement and aspect ratio is shown in Fig. 1(b2). The maximum differential optical chirality enhancement depends strongly on r/a, which can be very large at small r/a, and falls off exponentially as r/a increases.

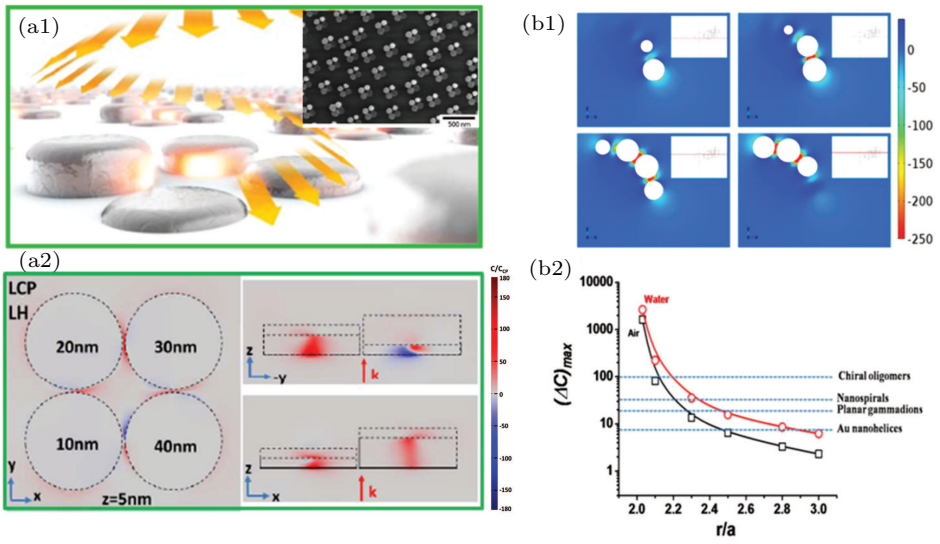


Fig. 1. (a1) Schematic and scanning electron microscope (SEM) image (inset) for silver tetramers. (a2) Simulated optical chirality enhancement factor of an RH silver tetramers in a vacuum on a glass substrate based on the finite element method (FEM) at 880 nm for LCP light.[20] (b1) Differential enhancement of optical chirality for various planes perpendicular to the helix axis containing four Au NPs ($a = 5$ nm and $r/a = 2.1$) embedded in water. The positions of the slices are shown in the inset (red lines). (b2) Plot of maximum possible magnitude of differential enhancement of optical chirality around the NP complex for different values of r/a.[21]

3.1.2. Planar chiral nanostructures

Planar chiral nanostructures refer to the objects that cannot be superimposed with their mirror images unless they are lifted from the plane. The advantage of planar nanostructures is that they are compatible with modern lithography techniques, which enables the precise location of nanostructures, helpful for the manipulation of interaction between electric and magnetic dipoles and the generation of uniform superchiral field.

Gammadion is a common planar chiral nanostructure for investigating the generation of superchiral field.[26–30] Many measurements and calculations on optical chirality of gammadion arrays have been demonstrated recently. The enhanced optical chirality around gammadion mainly located at the front and the back of the four arms. The drawback of gammadions is that the regions with enhanced optical chirality are at the same position and have the same sign for both incident RCP and LCP, but with different absolute values, as shown in Figs. 2(a1) and 2(a2). Therefore, there will be only a small change in optical chirality when the incident polarization is changed. This is not favorable for enantiomer sensing which measures the different response of chiral molecules to LCP and RCP. As an additional disadvantage, the enhancement is discontinuous in the space near gammadions. Experimentally, the near-field electromagnetic distribution of optical chirality nearby gammadions was measured using scanning near-field microscope (SNOM) under illumination of 633-nm He–Ne linearly polarized laser, as shown in Fig. 2(a3). Similar to theoretical results, the optical chirality is discontinuous in the space and strongly depends on position.

Compared with gammadions, nanospirals are much advanced for generating superchiral fields. The spiral features fewer sharp corners, as shown in Figs. 2(b1) and 2(b2), which allows for smoother distribution of optical chirality. Besides, each spiral features one and a half rotations, while a gammadion offers only one 90° kink at each arm. Under illumination, the optical chirality is different for incident LCP and RCP. LCP light leads to the ringlike region with enhanced chirality, while the enhanced region for RCP light is concentrated mainly in the center. Also, the signs of the chirality at the front and back of the spiral along the z direction are opposite for LCP and RCP light. Schnell *et al.* mapped chiral near-field distribution of nanospirals with scattering-type scanning near-field optical microscopy (s-SNOM) experimentally.[24] Figure 2(b3) shows images of the chiral optical near-field distribution for the right-wound nanospiral under illumination of LCP and RCP light respectively, which are quite in agreement with the simulated results.

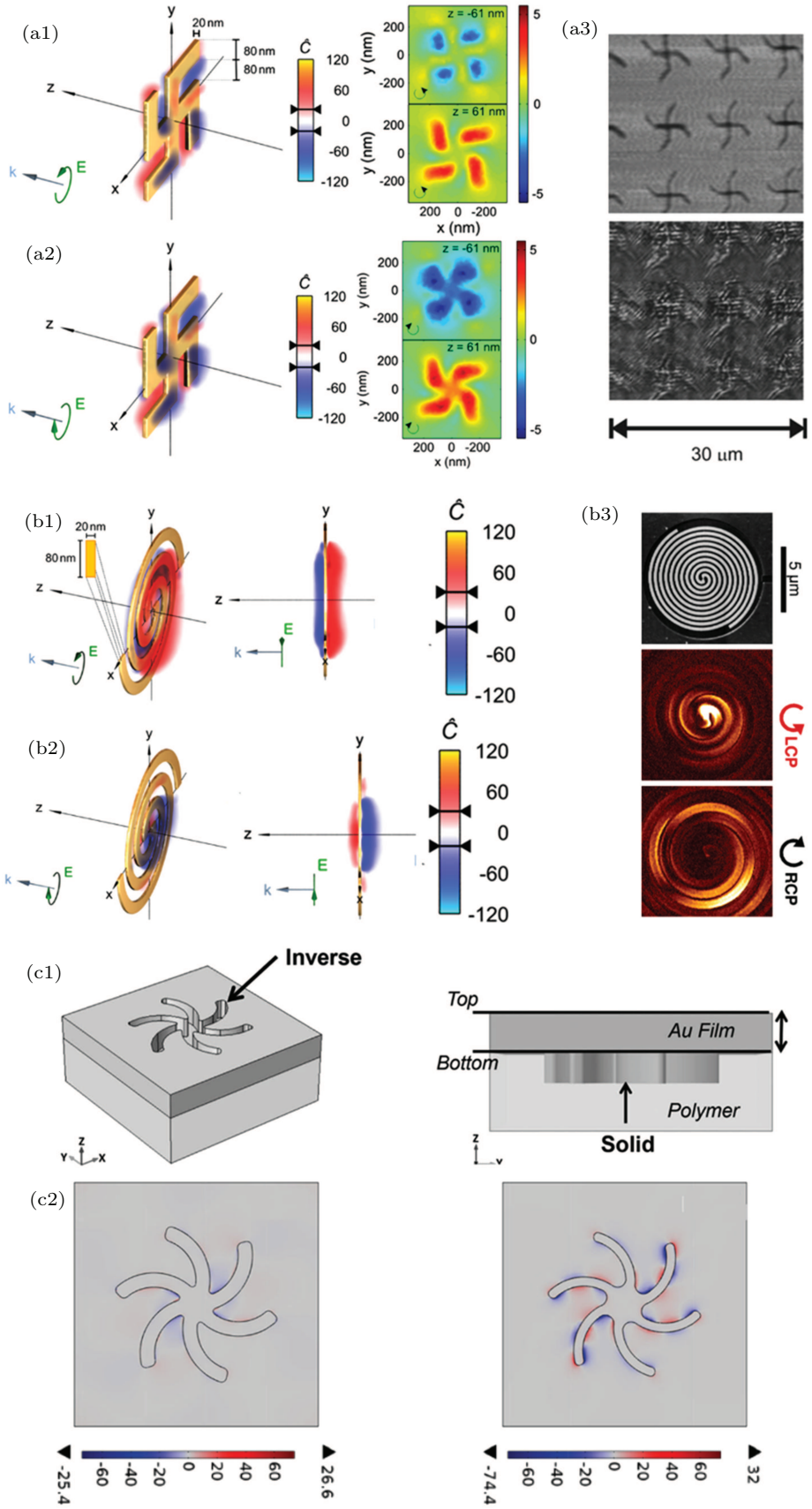


Fig. 2. (a1) Optical chirality enhancement by a planar gammadion structure illuminated with LCP. (a2) Optical chirality enhancement by a planar gammadion structure illuminated with RCP.[22] (a3) Near-field optical distributions above planar gammadions.[23] (b1) Optical chirality enhancement by a two-armed gold nano-spiral illuminated with LCP.[22] (b2) Optical chirality enhancement by a two-armed gold nano-spiral illuminated with RCP.[22] (b3) Topography images and experimental near-field amplitude images of the nano-spiral illuminated with LCP and RCP.[24] (c1) Perspective and side views of a solid-inversed plasmonic "shurikens". The thickness of gold film is shown as indicated. (c2) Different optical chiralities of shurikens with 30-nm and 100-nm gold films.[25]

In addition, figure 2(c1) shows a solid-inversed plasmonic "shuriken" structure which enables more explicit interaction between electric and magnetic dipoles in line with Babinet's principle. The shurikens were fabricated by depositing gold on nanostructured polycarbonate substrates that have "shuriken" shaped indentations.[25] This solid-inversed structure consists of a solid nanostructure and an identical shaped void structure above it, which enables symmetry equivalent electric and magnetic modes spatially located directly above each other, yielding strongly enhanced superchiral near field. When altering the thickness of gold films, the interaction between electric and magnetic modes can be manipulated, which provides a versatile approach to tune the optical chirality. For example, figure 2(c2) shows the different optical chiralities from the shurikens with 30-nm and 100-nm gold films.

Staggered nanoslits/nanorods can also be used to generate chiral electromagnetic fields.[31] Both nanoslits/nanorods are resonant when the wavelength of incident light is approximately twice the length of the nanoslits/nanorods. On resonance, a current maximum (and corresponding maximum in magnetic field) is found at the center of the nanorod. For a nanoslit, which is the complementary structure of the nanorod, high magnetic field toward the ends of the nanoslit and a maximal electric field in the center would arise.[32,33] If the two nanorods/nanoslits are shifted by half their length, the maxima of electric field and magnetic field, which exhibit a natural phase shift of $\pi/2$, overlap and thus maximize the electromagnetic chirality of the structure.[34] Similar to gammadions and nanospirals, the optical chirality changes sign from superstrate to substrate sides of the nanoslit arrays.

3.1.3. Three-dimensional chiral nanostructures

Compared to planar chiral systems, 3D chiral nanostructures offer more possibilities in optical chirality enhancement than the two-dimensional case. However, the studies on 3D nanostructures are still at an early stage because of the challenge in fabrication. State-of-the-art fabrication methods for 3D nanostructures include direct laser writing,[35] glancing angle deposition,[36,37] electron and ion–beam-induced deposition,[38–40] self-assembly,[41,42] *etc*.

Helical nanostructures, which possess chirality in 3D, have attracted much attention on generating superchiral fields.[43,48] Helical nanostructures can naturally meet the requirement of nonzero optical chirality — the electric and magnetic fields have parallel components that are out of phase, as shown in Fig. 3(a1).[43] Therefore, large regions with uniform and intense optical chirality inside the helix are expected. Helix has already been successfully fabricated in experiment.[39,40,49] For example, figure 3(a2) shows the SEM image of helices fabricated with focused electron beam induced deposition.[35] However, there is a drawback for the single helix that a larger pitch results in increase of the absolute value of optical chirality, but meanwhile weak confinement of the field. This leads to a trade-off between strength, confinement, and net chirality of the generated chiral fields. Adding additional helices can solve this problem and obtain both better confinement and stronger enhanced optical chirality.[43] The dimensions of helix can be tuned to be feasible for current fabrication technologies. Triple-helical nanowires have been successfully fabricated in experiment with focused ion beam-induced deposition.[47] The optical chirality is strong and uniform inside the four-helix structure and can be almost 2 orders of magnitude higher than CPL, as shown in Fig. 3(b2).[43]

Many works have been done to design alternate 3D structures that are easy to be fabricated. Tseng *et al.* proposed an easy method to fabricate 3D Archimedean spiral with homogeneous and highly enhanced broadband near-field optical chirality.[44] The 3D Archimedean spirals were fabricated firstly with gallium focused-ion beam (FIB) to mill Archimedean spiral patterns in a freestanding Au/Si_3N_4 bilayer film (Au layer: 50 nm; Si_3N_4: 50 nm). Because of the stress and defects introduced by FIB, freshly milled planar spirals will stretch themselves immediately out of the plane to form 3D spirals, as show in Fig. 3(c1). The near-field optical chirality enhancement along the central axis of the spiral (marked with a black line in Fig. 3(c2)) is plotted with respective to wavelength in Fig. 3(c3). As can be seen, the 3D Archimedean spiral exhibits a highly enhanced (enhancement factor up to 20), stably localized, and broadband (2 μm–8 μm) optical chirality inside the spiral.

Layered structures that mimic helix can also be used to simplify the fabrication process and simultaneously hold enhanced optical chirality. Figures 3(d1) and 3(d2) show a structure consisting of diagonal nanoslits in a metallic film on top of a mirror, which is simplified from nanohelices.[45] This diagonal-slit structure can be fabricated easily by conventional electron-beam lithography, because only one nanostructured layer is needed. The simplification process is depicted in Fig. 3(d1). Starting from four intertwined helices, the helices are replaced firstly by a two-layered design composed of diagonal stripes. Then the lower layer is replaced by a mirror. As a last step, the upper layer is replaced by its inverse structure. Optical chirality depends strongly on the distance between the two layers. At proper distance, strong chiral near-field with only one handedness can be generated within the nanoslit, and the enhancement factor can be 1 order of magnitude, as shown in Fig. 3(d2). Besides, the fields with enhanced optical chirality within nanoslits are easy to be accessed for chiral molecules. Figure 3(e) displays a bilayer structure that mimics a helix, which is called chiral oligomer.[22] Each layer of the oligomer consists of three gold disks arranged in L-shape, with the second layer twisted by 90° with respect to

the first. Nanofabrication of such stacking structures is relatively well-established. A continuous region with consistent enhanced optical chirality is located around the two disks at the bottom left of the oligomer, as shown in Fig. 3(e). Compared to CPL, its optical chirality can be enhanced more than 100 times. Stacked and twisted plasmonic split-ring resonators can also be used for optical chirality enhancement, as shown in Fig. 3(f1).[22] The strongest enhancement is located in the layer between the two resonators. The twist angle could be used to tune the optical chirality. The SEM image of experimentally fabricated twisted split-ring resonators is shown in Fig. 3(f2).[46]

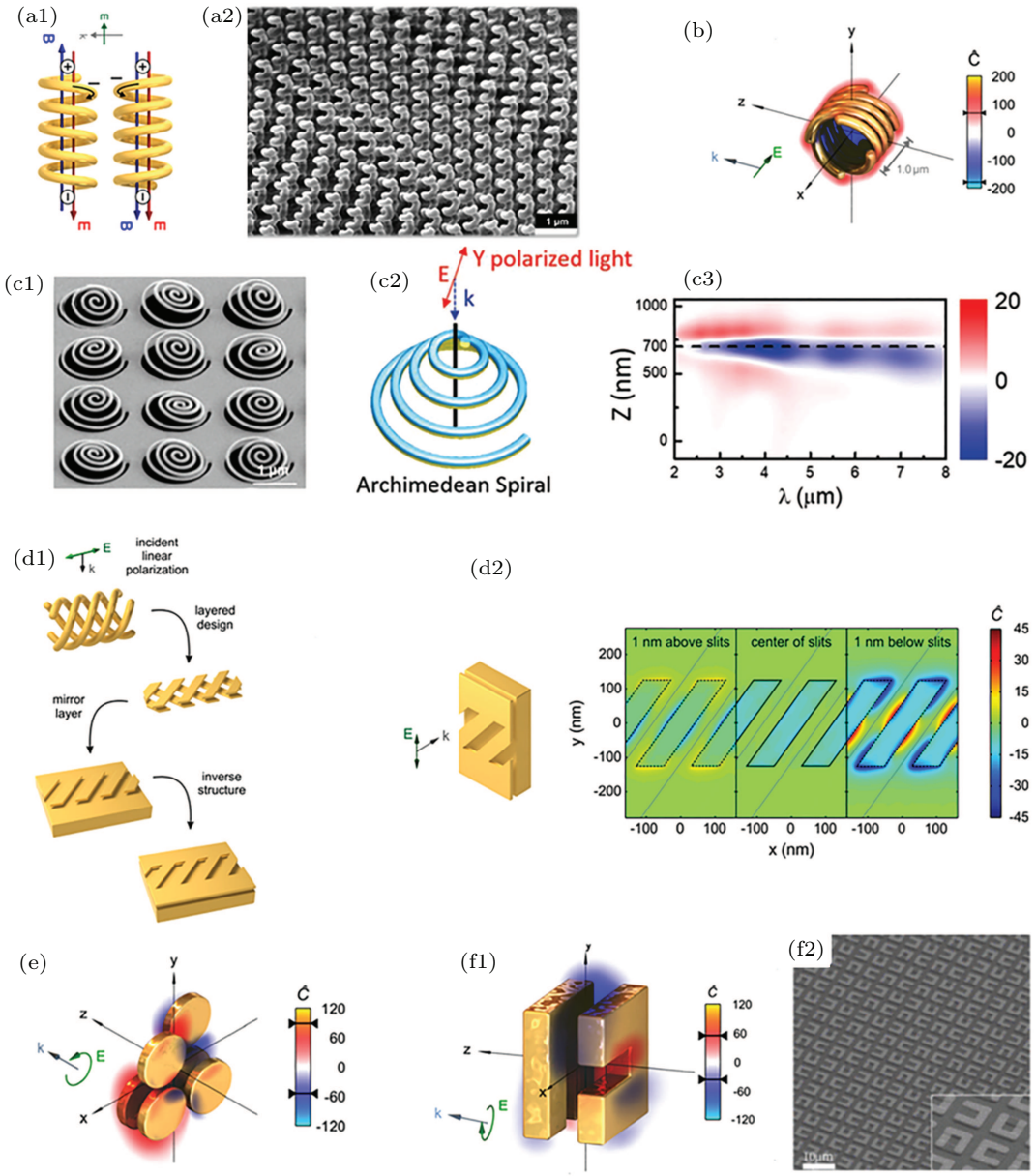


Fig. 3. (a1) The fundamental mode of a helical plasmonic nanoantenna with nonorthogonal electric and magnetic dipole moments. The electric (red) and magnetic (blue) field vectors are mainly parallel within the structure.[43] (a2) Oblique SEM image of helix structure fabricated based on focused electron beam induced deposition.[35] (b) Map of strong chiral field with only one handedness inside the four-helix structure.[43] (c1) Tilted SEM images of the 3D Archimedean spirals. (c2) The schematic of a 3D Archimedean spiral. (c3) Optical chirality of a 3D Archimedean spiral.[44] (d1) Schematic of steps to optimize a complex design of intertwined helices to diagonal nanoslits. (d2) Distribution of chiral near-field generated by diagonal-slit structures with a 20 nm layer distance.[45] (e) Optical chirality enhancement of the chiral oligomer for incident LCP at a wavelength of 900 nm.[22] (f1) Optical chirality enhancement induced by RCP as incident polarizations at wavelength 1.34 μm.[22] (f2) SEM image of double-layer of U-shaped gold nanostructures. Details of the double-layer structure can be identified from the inset.[46]

3.2. Ultrasensitive detection of chiral molecules based on chiral nanostructures

Superchiral fields generated by chiral nanostructures make them feasible for ultrasensitive chiroptical measurement. The basis of most ultrasensitive biosensing utilizing chiral nanostructures is the wavelength dependence of plasmonic resonance on the dielectric environment.[50] When chiral molecules interact with the superchiral field, the effective refractive indices for chiral molecules adsorbed on left-handed (LH) and right-handed (RH) chiral nanostructures are differ-

ent, which will result in different resonance wavelength shifts for LH and RH nanostructures coated with the same chiral molecules. The shift of different resonance wavelengths is a direct analogue to the CD signal in conventional chiroptical spectroscopic measurement.

For gammadions, CD signals of bare LH and RH gammadions display essentially mirror CD spectra to each other.[54] When adsorbed chiral molecular layers, the wavelength shift of LSPRs for LH gammadion ($\Delta\lambda_{\mathrm{RH}}$) and RH gammadion ($\Delta\lambda_{\mathrm{LH}}$) is different, indicating the sensing capability of chiral molecules. Besides, this shift dissymmetry ($\Delta\Delta\lambda = \Delta\lambda_{\mathrm{LH}} - \Delta\lambda_{\mathrm{RR}}$) is influenced by the structures of absorbed chiral molecules, with different shifts for different chiral species. The magnitude of this dissymmetry for β-sheet protein is the largest, and is about 10^6 times than typically observed dissymmetry measured with CPL. The authors attributed this large dissymmetry to molecular quadrupolar contribution. For β-sheet proteins, because of the planarity of the structures, the molecules adsorbed on the gammadions will be anisotropic, and the enhanced quadrupolar contributions to CD spectrum may give rise to large dissymmetry in the CD spectral shift. As for the α-helix structures, owing to the number and broad spatial distribution, they will be isotropically distributed with respect to the gammadions, and the quadrupolar contribution will be small. Thus, in addition to detect presence of chiral molecules, gammadions can also be used for the determination of molecule structures.

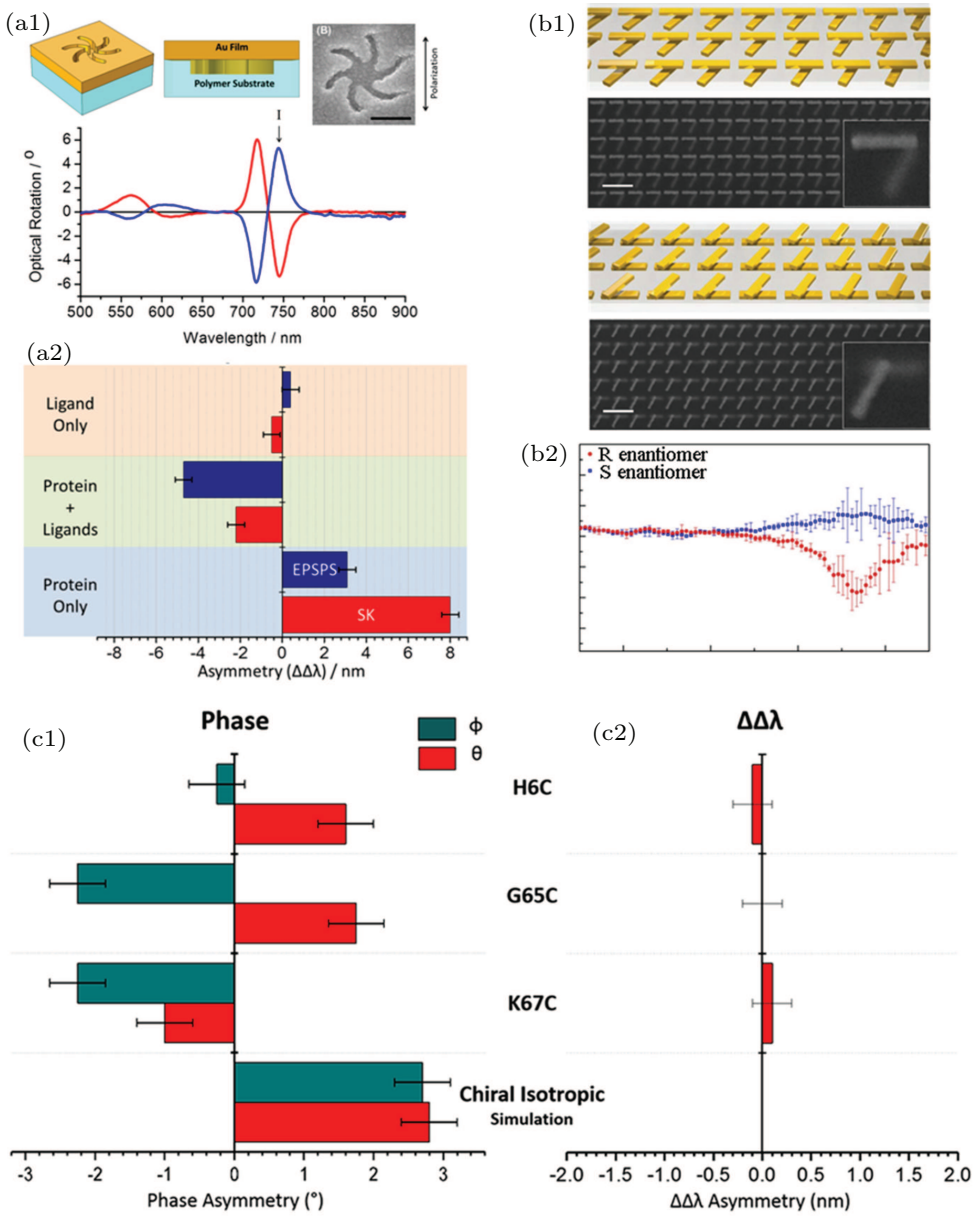


Fig. 4. (a1) Graphical description of a single LH shuriken structure and ORD spectrums for bare LH and RH shuriken structures. (a2) $\Delta\Delta\lambda$ values for ligand only, protein only and protein with ligand-induced conformation adsorbed on shuriken structures.[51] (b1) Schematic and SEM images of the twisted plasmonic metamaterials. (b2) CD signals removed the background CD. The curves show clear opposite signs for R and S enantiomers.[52] (c1) Asymmetry in phase parameters ($\Delta\Delta\theta$ and $\Delta\Delta\Phi$) for the three proteins and the simulated isotropic chiral layer. (c2) $\Delta\Delta\lambda$ values for the three proteins.[53]

Shuriken structures can also be used for the chiral molecular detection and structure discriminating.[51,55] Without molecules, ORD spectrums for LH and RH shuriken structures show expected mirror image, as shown in Fig. 4(a1). Similar to gammadions, the wavelength shifts for the LH and RH nanostructures are different when adsorbed pictogram level chiral molecules. In addition to roughly determinate the chiral molecule, shuriken structures can also rapidly characterize ligand-induced high order (tertiary/quaternary) changes in structure for biological macromolecules. When less than 100 picogram ligand only, protein only and protein with ligand-induced conformation changes were respectively put on the surface of shurikens, $\Delta\Delta\lambda$ for each surface coverage is different, indicating the great sensitivity to detect ligand-induced conformational change, as shown in Fig. 4(a2). In addition, because that functionally important protein-protein interactions result in a structurally well-defined complex, while nonspecific interactions produce random aggregates, the structural order of protein-protein products can be used to discriminate between functionally protein-protein interactions and nonspecific protein-protein interactions. Based on the phenomenon that structurally anisotropic ordered protein produce larger asymmetries between the chiroptical spectrums of LH and RH structures than isotropic disordered ones, chiral plasmonic nanostructures provide a rapid method to discriminate functionally important protein-protein interactions.[56]

However, further improvement of the detection sensitivity based on resonance wavelength shift is difficult because the final spectrum is in combined with the CD signal of background chiral nanostructure. Introducing molecules in the near field of chiral plasmonic nanostructures can also result in resonance wavelength shift due to refractive index changes, regardless of the handedness of molecules. This makes the direct detection of weak molecular chirality difficult with resonance wavelength shifts. Zhao *et al.* proposed a plasmonic 'twisted' material to isolate molecular CD response from the large background CD signal, enabling high sensitivity detection of chiral molecules down to zeptomole levels.[52] The SEM and schematic images for a pair of $+/-60^\circ$ twisted metamaterials are shown in Fig. 4(b1). To cancel contribution of substrate chiral nanostructures, the CD signals for $+60^\circ$ and -60° twisted metamaterials adsorbed with same molecules were summed. After proper post-processing, isolated CD signals of chiral molecules can be obtained even when there are small fabrication imperfections in substrate metamaterials, as shown in Fig. 4(b2). This platform provides a method for drastically enhance molecular chirality detection sensitivity without relying on any spectrum shift.

In addition, phase retardation effects were also used to increase chiral sensing sensitivity.[53] Phase retardation refers to the phase different propagating from specially different point of the nanostructure, which is sensitive to interactions between chiral near fields and chiral molecules. For the LH and RH nanostructures adsorbed with same molecules, the phase retardation is asymmetry, which can be used for the chiral sensing. Solid-inverse shurikens were used as the chiral substrate, and three structurally similar proteins were adsorbed on the LH and RH shurikens. Experimental reflectance spectrums of the systems were fit to extract the phase parameters. As shown in Fig. 4(c1), $\Delta\Delta\theta$ and $\Delta\Delta\Phi$ which account for the phase retardation differ significantly for the three proteins, while $\Delta\Delta\lambda$ values for these proteins are small and within the experimental error (Fig. 4(c2)), demonstrating the greater incisiveness of asymmetries in phase to the structure of biointerfaces.

3.3. Competition of chiroptical effect caused by nanostructure and chiral molecules

The drawback of ultrasensitive chiral sensing based on chiral nanostructures is that chiral nanostructures have their own geometrical chiral signals even in the absence of chiral molecules, and the total CD results are usually combined with the background geometrical CD signals. It is hard to distinguish molecular CD from the geometrical chirality.[57] Figs. 5(a) and 5(b) display molecule-induced CD signals and the background structure CD for Au spheroid chiral trimers caused by nanoparticles dislocation and rotating respectively. The dashed/dotted lines represent structure chirality/molecule-induced CD signals respectively, and the total CD signals are

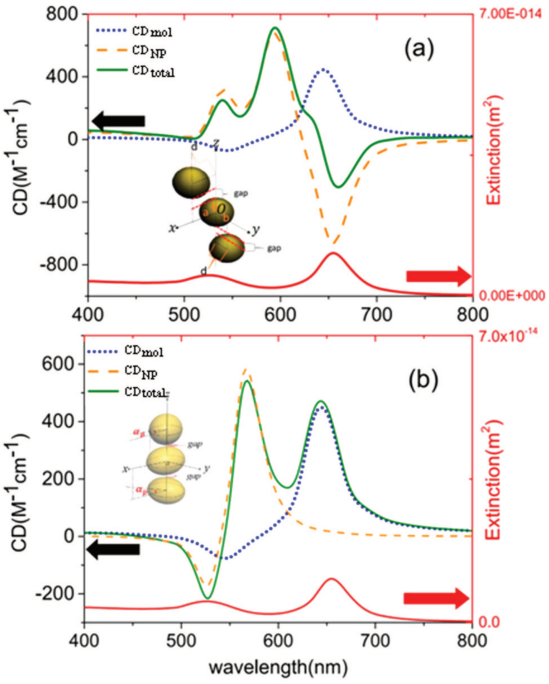


Fig. 5. (a) Calculated CD and extinction spectrums as a function of wavelength for the Au spheroid chiral trimer caused by dislocation of nanoparticles. Here the long axis $a = 17.5$ nm, short axis $b = 17$ nm, and $d_1 = d_2 = 1$ nm. One molecule is placed at $x = 0.0$, $y = 0.0$, and $z = 17.5$ nm, the other is at $x = 0.0$, $y = 0.0$, and $z = -17.5$ nm. (b) Calculated CD and extinction spectrums as a function of wavelength for the Au spheroid chiral trimer caused by rotating nanoparticles. Here the long axis $a = 17.5$ nm, short axis $b = 17$ nm, rotation angle $\alpha_p = 0.0025^\circ$, and gap = 1 nm. The solid line, dashed line, and dotted line represent the total CD, the structure chirality, and the molecule-induced plasmon chirality, respectively; the red line is extinction spectrum.[57]

described by solid lines. As seen in Fig. 5(a), the molecular and background CD signal overlapped with each other, and total CD cannot represent the molecule-induced CD signal. Only for the trimer in Fig. 5(b), the CD background signal is weak of at the wavelength of molecule-induced CD signal, the total CD signal can be used to represent the molecule-induced chirality.

4. Superchiral fields generated by achiral nanostructures and the corresponding chiral sensing

In addition to chiral nanostructures, achiral nanostructures can also generate superchiral fields. Besides, achiral nanostructures can easily eliminate the influence of background CD signals. Intensive works have been devoted to superchiral fields generated by achiral nanostructures and their corresponding chiral sensing.

4.1. Superchiral fields generated by achiral nanostructures

We start from single achiral nanoparticle. The optical chirality of a 10-nm radius silver sphere illuminated by circularly polarized plane wave is shown in Fig. 6(a1).[58] Extinction cross section of the silver sphere (blue line), optical chirality enhancement factor ($f(r) = C/|C_{\rm cpl}|$) on a point 1 nm above the sphere at the wavelength of 359 nm, and averaged optical chirality enhancement factor ($f_{\rm avg} = \int f(r)\,{\rm d}S/(4\pi r^2)$) over the surface of silver sphere (red line) were plotted. The right panel in Fig. 6(a1) plotted the distribution of optical chirality along the surface 1 nm above the surface of silver nanosphere at the wavelength of 359 nm. Apparently, the localized surface plasmon resonance occurs at a wavelength of $\lambda = 355$ nm. When $\lambda = 359$ nm, slightly off the plasmonic resonance, the phase of scattered field will not be $\pi/2$ delayed with respect to the incoming magnetic field, thus a local enhancement of optical chiraliry can be obtained, as shown in the green line in Fig. 6(a1). However, the enhancement is not uniform for silver nanosphere, and $f(r)$ is both positively and negatively enhanced in different regions, as shown in the right panel of Fig. 6(a1). Thus, the average enhancement over the surface of silver sphere is found to be $f_{\rm avg} = 1$. High refractive index dielectric nanoparticles, however, which support both electric and magnetic Mie resonances in the visible and infrared spectrum,[63,64] can achieve both local and global enhancements of the optical chirality. The left panel of Fig. 6(a2) plots optical chirality enhancement factor $f(r)$ calculated at a point 1 nm above a silicon nanosphere with radius of 75 nm (green line), and the average enhancement $f_{\rm avg}$ (red line). Unlike silver nanosphere, the averaged chiral field is enhanced compared to $C_{\rm cpl}$. The local enhanced factor $f(r)$ and the average enhancement $f_{\rm avg}$ both reached a maximum at the wavelength of 625 nm. The three-dimensional distribution of the optical chirality enhanced factor $f(r)$ on the surface 1 nm above the sphere at this wavelength is shown in the right panel of Fig. 6(a2). $f(r)$ is positive all over the surface, and $f_{\rm avg}$ is about 1 order of magnitude larger than that of CPL, demonstrating the ability of CD enhancement via isolated nanoparticles supporting both electric and magnetic dipoles.

For closely packed nanoparticles, strong and uniform superchiral field can be generated in hot spots.[59,65–71] Figure 6(b1) displays the optical chirality for dimers of silicon and Au nanodisks.[59] Uniform superchiral near-field can be achieved for Si nanodisk dimers excited with linearly polarized light because of the simultaneously excited electric and magnetic dipole resonances. In addition, the optical chirality of Si nanodisk dimers is much stronger than Au nanodisk dimers, as shown in Fig. 6(b1) (The red/black dots in Fig. 6(b1) correspond to the chiral near-field enhancement factors for Au/Si nanodisk dimers with different interparticle gaps). The analysis in Fig. 6(b2) explains the reason for this difference in chirality enhancement: with the almost identical electric field for Si and Au nanodisk dimers, the H-field intensity is 2–5 orders of magnitude higher for Si nanodisk dimers. This confirms that the significant enhancement of the optical chirality in Si nanodisk dimers comes from the enhanced magnetic field provided by the magnetic dipole resonance.

It is challenge for metal nanoparticles to generate uniform surperchiral over a large region because of their magnetic dipole resonances are either weak or far away from electric dipole plasmon resonances.[72–76] High refractive index dielectric nanoparticles such as silicon nanoparticles can yield a globally uniform enhanced optical chirality with both the magnetic and electric resonances, but the chiral field enhancement is usually modest and confined in small volume. People have done a lot of work to generate uniform and strongly enhanced chirality over a large region based on achiral metamaterials.[60–62,74,77] Engineered plasmonic nanostructures such as metal-insulator-metal,[77] metallic split-ring resonators[60] and complementary structures can provide uniform superchiral field with simultaneously excited electric and magnetic resonances. For example, figure 6(c) displays achiral gold double split rings which can sustain magneto-electric coupling. The spatial distribution of the electric and magnetic fields guarantees the perpendicular components and the intrinsic phase difference for these fields, which can result in an extended enhanced optical chirality inside the inner ring of double split ring resonators.[60] Besides, dielectric metasurfaces,[78–81] such as hollow silicon disk arrays, diamond nanodisks, *etc*., were also used to generate uniform and greatly enhanced optical chirality.

Negative-index metamaterials are also used to generate uniform globally enhanced optical chirality. Figure 6(d) dis-

plays a negative-index metamaterial stacked by double-fishnet layers.[61] In the cavity of this structure, uniform-sign superchiral field can be generated over the entire region. The mechanism of the superchiral field generation of this negative-index material is the simultaneous excitation of the strong electric and magnetic fields in the longitudinal direction, satisfying the parallel and out of phase condition for the generation of large optical chirality.

In addition to tuning electronic and magnetic resonance to generate superchiral field, figure 6(e) displays a new method to generate uniform superchiral fields based on radiation vector exceptional points (EP).[62] This radiation vector EP is realized by suitably tuning the coupling strength and radiation losses for a pair of orthogonal polarization modes in the Si_3N_4 photonic crystal slab. At the vector EP, these two orthogonal polarization modes are nearly coupled to the opposite output ports, and the modal electric fields possess a large component parallel to the magnetic fields. Strong uniform superchiral field can be generated at the vector EP with excitation of two light illuminating from opposite directions, as shown in Fig. 6(e1). Figure 6(e2) displays the averaged enhancement of optical chirality in the cylindrical hole of the photonic crystal slab with different thicknesses. In the system sustaining the vector EP, maximal optical chirality appears (blue line, thickness is 154.2 nm). The corresponding distribution of superchiral field, which is strong and homogeneous, is shown in Fig. 6(e3).

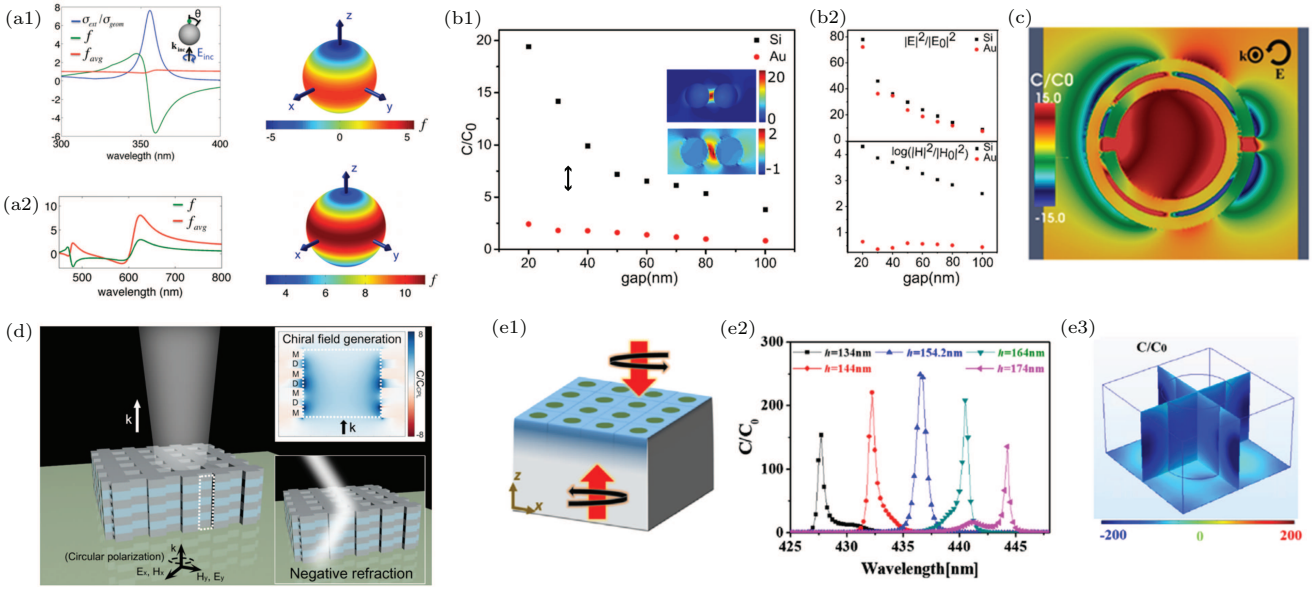


Fig. 6. (a1) Optical chirality enhancement of a 10-nm radius silver nanosphere. Left panle: geometrically normalized extinction cross section (blue line), CD enhancement factor $f(r)$ at a point 1 nm on top of the sphere (green line), and averaged CD enhancement factor f_{avg} over a sphere covering the particle (red line). Right panel: CD enhancement factor $f(r)$ plotted over a surface 1 nm above the silver sphere at $\lambda = 359$ nm. (a2) Optical chirality enhancement of a 75-nm radius silicon nanosphere. Left panel: CD enhancement factor $f(r)$ at a point 1 nm above the sphere (green line), and averaged CD enhancement factor f_{avg} over a three-dimensional surface (1 nm above the sphere) covering the particle (red line). Right panel: distribution of CD enhancement factor $f(r)$ over a surface 1 nm above the silicon sphere at the wavelength of 625 nm.[58] (b1) Optical chirality enhancement for Si nanodisk dimer (black square, $D = 140$ nm, $h = 100$ nm) and Au nanodisk dimer (red circle, $D = 100$ nm, $h = 100$ nm) as a function of gap width. D and h are the diameter and height of the nanodisks. Inset: chirality density maps for Si dimer (top) and Au dimer (bottom) with gap width of 20 nm. (b2) Electric field intensity enhancement (top) and magnetic field intensity enhancement (bottom) for Si dimer (black square) and Au nanodisk dimer (red circle). The field intensities were obtained by averaging over a square with side-length centered in the gap.[59] (c) Optical chirality distribution for gold double split rings. A uniform-sign enhanced chiral field is generated inside inner ring.[60] (d) Schematic diagram of a double-fishnet structure. The inset shows a spatial distribution of the optical chirality under normally incident CPL.[61] (e1) The scheme to generate the superchiral field at the radiation vector exceptional points (EP) using two beams of CPL exciting the system from opposite directions. (e2) The averaged enhancement optical chirality in the cylindrical hole with different thicknesses. The blue line corresponds to the structure sustaining EP with $h = 154.2$ nm. The black, red, green, and pink lines correspond to cases deviating from the vector EP. (e3) Near-field distribution of optical chirality near the photonic crystal slab at the vector EP under two beams of excitation from opposite directions.[62]

4.2. Ultrasensitive detection of chiral molecules based on achiral nanostructures

The superchiral field generated by achiral nanostructures paves the way for ultrasensitive chiral sensing. Unlike chiral structures, achiral nanostructures have no chiral signals. The basis of most ultrasensitive biosensing utilizing achiral nanostructures is the enhancement of optical chirality. The large superchiral field will greatly enhance chiral signals of chiral molecules placed on achiral nanostructures. Both achiral nanoparticle clusters and metasurfaces were studied in the ultrasensitive chiral detection.

4.2.1. Achiral nanoparticle clusters

4.2.1.1. Metal nanoparticles

One of the first experimentally strong plasmonic CD enhancement was reported for a complex system combined of colloidal silver nanoparticles and chromophore molecules.[89] The wavelength of molecular adsorption is the same as the

localized surface plasmon resonance of silver nanoparticles. Finally, the CD signal of this system increased two orders of magnitude contrasted to pure molecules.

Theory studies on the mechanism of the plasmonic CD enhancement were promoted by these results.[90–92] It has been shown that coupling of a chiral molecule and a small achiral plasmonic nanoparticle can dramatically enhance the molecular CD signal both at the wavelength of molecular adsorption and the plasmon resonance. Two mechanisms for this enhancement were identified. The first is the plasmon-induced change in the angle between effective electric and magnetic dipoles of molecules, which will amplify the molecular CD signal. The second is that chiral currents will be induced inside the metal nanoparticles by the dipole of the chiral molecule, resulting in a new CD peak in the visible wavelength. The CD enhancement is strongly depended on the separation Δ between molecules and metal nanoparticles, and decreases with the separation Δ as Δ^{-3}.

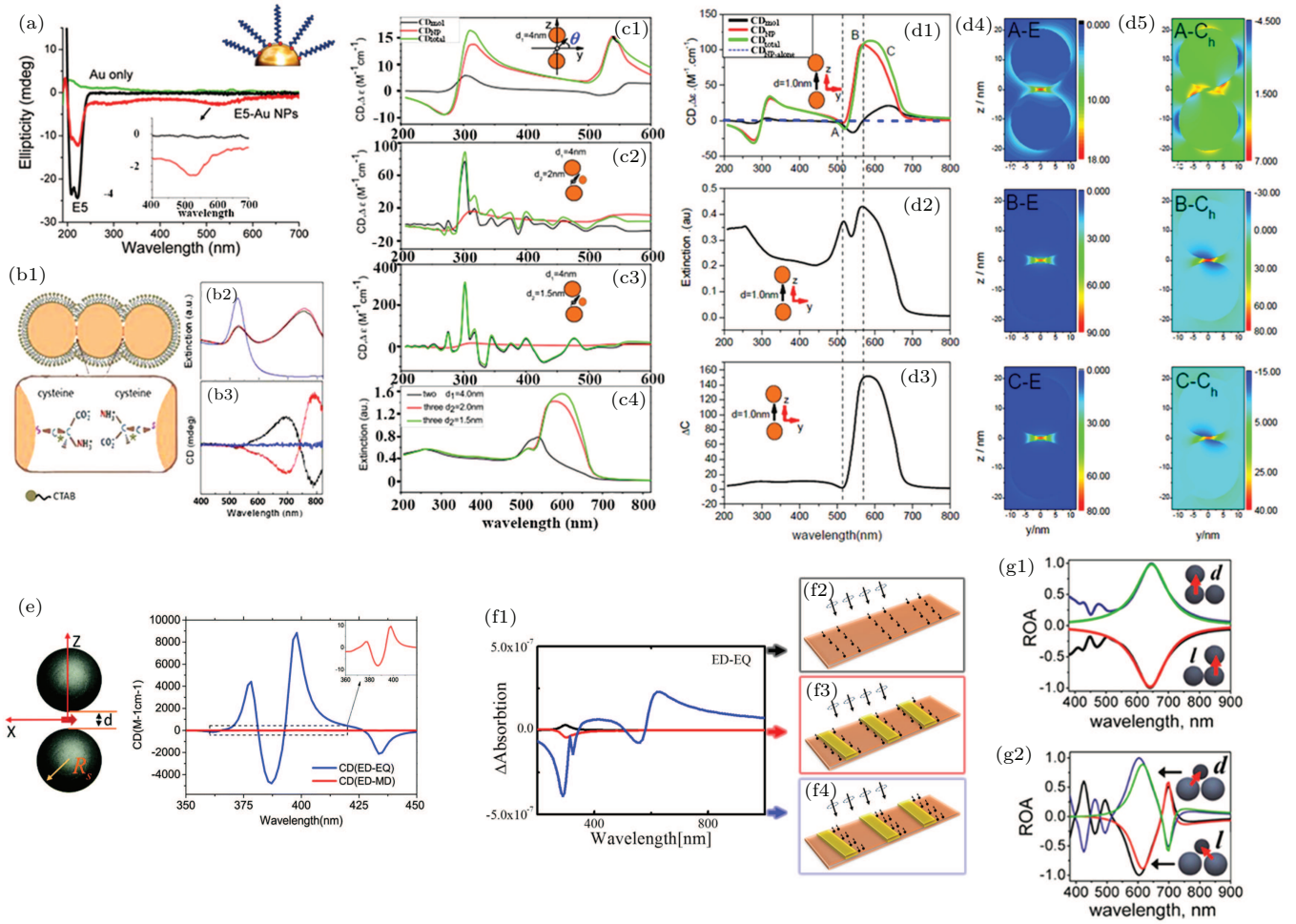


Fig. 7. (a) CD spectra of gold nanoparticles with or without E5 peptide. The green/red/black line corresponds to the CD spectrum of Au nanoparticles only/E5 molecules/E5-gold nanoparticle complex system, respectively. Inset: illustration of gold nanoparticle surface covalent linked to the E5 peptide via the thiol linkage (red circle).[82] (b1) Schematics of cysteine-mediated linear assembly of gold nanospheres (GNSs). [(b2) and (b3)] Vis/NIR extinction spectrums (b2) and corresponding CD spectrums (b3) from the isolated GNSs (blue solid line), the L-cysteine modified GNSs (black solid line) and D-cysteine modified GNSs (red solid line) clusters. The concentration of L- and D-cysteine linkers is of $\sim 2.3 \times 10^{-6}$ M.[83] (c1)–(c3) Calculated CD signals as a function of wavelength for molecule–nanosphere complexes with two spheres (c1), two large spheres and one small sphere with $d_2 = 2$ nm (c2), two large spheres and one small sphere with $d_2 = 1.5$ nm (c3). Here d_2 represent the distance between the molecule and small sphere, and $d_1 = 4$ nm is the distance between two large spheres. The radii of two large Au spheres are taken as 17.5 nm, the radius for small Au sphere is taken as 4 nm. In inset, $\theta = \pi/3$ represents the angle between the orientation of molecular dipole and y axis. (c4) Calculated extinctions for Au nanospheres dimer and trimer systems.[84] (d1)–(d3) Calculated CD signals (d1), extinction spectrums (d2), and superchiral fields (d3) as a function of wavelength for molecule–Au-dimer complexes with the separation between two spheres set as 1.0 nm. The radii of the two Au spheres are taken as 10.0 nm. (d4) Panels A–E, B–E, and C–E represent the spatial profiles of the electric field amplitudes in the yz plane at the A, B, and C points in panel (d1). (d5) Panels A–C_h, B–C_h, and C–C_h are the corresponding optical chiralities. Insets show the position and orientation of a molecular dipole at a plasmonic hot spot.[85] (e) Left panel: schematics of the system with a Ag dimer and a chiral molecule. The radius of Ag nanosphere is 15 nm, and the distance in the dimer is $d = 1$ nm. Right panel: CD(ED-MD) and CD(ED-EQ) as a function of wavelength for the system in the left panel.[86] (f1)–(f4) CD spectrum for the oriented chiral molecule systems. (f1) The black, red and blue lines present the CD signal for the pure oriented chiral medium (as plotted in panel (f2)), chiral medium with the symmetric distribution around the nanoribbon (as plotted in panel (f3)), and chiral medium with the asymmetric distribution around the nanoribbon (as plotted in panel (f4)), respectively.[87] (g1) ROA signals of the L-shaped trimer with d and l configurations. (g2) ROA signals of trimers of Au nanospheres that have different sizes, with d and l configurations. Black and blue lines are calculated from electromagnetic simulation; the red and green line are calculated from the harmonic oscillator model. The insets are the schematic diagrams of the considered trimers.[88]

Later experimental works subsequently proved these theories.[82,93–98] Figure 7(a) plots the schematic image of the peptide-functionalized gold nanoparticles and the corresponding CD spectrums. The green/red/black line corresponds to the CD spectrum of Au nanoparticles only/E5 molecules/E5-gold nanoparticle complex system, respectively. A new strong visible CD signal can be observed at the wavelength of about 520 nm, which corresponds to the gold nanoparticle's surface plasmon resonance frequency.[82] Similar results were obtained for a bilayer of riboflavin 5′-monophosphate and polylysine molecules adsorbed on gold island films.[94] By carefully control the distance between the molecules and gold nanoparticles, the near-field enhancement of the induced CD signal was confirmed.

Stronger molecular enhancement was predicted for plasmonic "hotspots" located in gaps of nanoparticle aggregations.[99–101] In experiment, CD enhancement was observed in different aggregated systems, such as oligonucleotide-conjugated spherical gold nanoparticles,[102] cysteine-modified gold nanorods, and nanospheres,[83,103–105] as well as cholate-coated silver nanoparticles.[106] The CD enhancement for cysteine-modified gold nanosphere clusters was shown in Fig. 7(b1).[83] The extinction spectrums of isolated gold nanospheres (blue line), L-cysteine modified gold nanospheres (black line) and R-cysteine modified gold nanospheres (red line) are plotted in Fig. 7(b2). A new plasmon resonant appears at longer wavelength for cysteine linked clusters because of the strong near-field plasmonic coupling between adjacent particles. The blue/black/red line in Fig. 7(b3) represents CD signal of isolated gold nanospheres/L-cysteine modified gold nanospheres/R-cysteine modified gold nanospheres, respectively. Coincided with the resonant, around 2 orders of magnitude CD signal amplification in the visible region was observed.

It is not necessary for the absorbed chiral molecules to be in resonant with the metal nanoparticle plasmon to enhance the CD signal. However, for the system with matched molecular absorption and plasmon resonance wavelength, the CD enhancement effect will be stronger, suggesting the application of ultrasensitive chiral sensing in ultraviolet (UV) region.[84,94] In addition, Liu *et al.* demonstrated a new way to strongly enhance CD signal in UV region using plasmonic nanoparticle clusters.[84] Figures 7(c1)–7(c4) display the calculated CD signals and extinction spectrums for these molecule-nanoparticle cluster complexes. The black/red/green line corresponds to molecule CD/nanoparticles CD/the total CD respectively. Figure 7(c1) displays CD signals for the complex combined a molecule and Au nanosphere dimer. The resonance of molecules is at $\lambda = 300$ nm, and the plasmon resonance for Au sphere is larger than 520 nm (black line in Fig. 7(c4)). For Au nanospheres dimer in Fig. 7(c1), CD signals both at the wavelength of molecular excitation and the plasmon resonance for the dimer experience a small enhancement, in agreement with previous results. When a third small Au sphere is placed near the dimer, molecular CD (black line) is dramatically enhanced while the CD signal of nanoparticle clusters almost unchanged, resulting in a large total CD enhancement at the wavelength of 300 nm. The CD signal is improved 10 times when $d_2 = 2$ nm, and it reaches 40 times at $d_2 = 1.5$ nm (as shown in Figs. 7(c2) and 7(c3), d_2 is the distance between molecule and the third sphere). In addition, the enhancement is depended on the orientation of molecular. 2 orders of magnitude CD enhancement can be realized in UV region at small molecular orientation angle. This large CD enhancement was created by nanostructures induced modification in matrix elements of field-enhancement matrices, different from the previous reported plasmon-resonance-enhanced CD phenomenon.

People used to think that the main factor determining the molecular CD amplification and transfer in the hotspot is the enhanced electromagnetic field. Liu *et al.* demonstrated that it is the strong superchiral field in the hotspot, rather than the electromagnetic field, corresponds directly to the CD enhancement. Figures 7(d1), 7(d2), and 7(d3) show CD, extinction, and optical chirality spectrums for the hybrid system composed of a chiral molecule and an Au-dimer (the radii of Au sphere is 10 nm, the distance is 1 nm). The CD and extinction spectrums are not consistent with each other, with the scattering resonance peak appears at the wavelength of 520 nm, while the CD signal is near zero at this point, as shown in Figs. 7(d1) and 7(d2). In contrast, the signs and strength always stay one-to-one consistent for the superchiral field and CD spectrum. Figures 7(d4) and 7(d5) display the distribution of the electric field intensity and optical chirality at points A, B, and C in Fig. 7(d1), and the CD signal at each point also corresponds to its optical chirality. Thus, it is the optical chirality, instead of its EM field enhancement, plays a crucial role in the CD enhancement, breaking the preconception that the local field intensity at the hot spot is directly correlated to the plasmon-induced CD strength. This theory is in a good agreement with experimental results. With the CD signals shown in Fig. 7(b3) as an example,[83] the CD signal is near zero at the peak position of the extinction marked in Fig. 7(b2), inferring that the higher local field enhancement does not necessarily corresponds to a stronger CD.

In addition, there are often unexpectedly large CD signals, far beyond theoretical prediction, exported in experiments. Besides, the induced CD signal is sensitive to the orientation of the transition dipole moments of the adsorbed molecule, which can be inverted by the inversion of chiral molecule's orientation.[86,87,107] These experimental phenomena can be well understood by considering the contribution of molecular electric quadrupole.[86] Most theories on plasmon-induced CD are based on the dipole approximation (CD(ED-MD)), and the electric quadrupolar contribution (CD(ED-EQ))

is generally neglected. In fact, for molecules possess preferential orientations, CD(ED-EQ) plays a key role. Figure 7(e) displays the CD(ED-EQ) and CD(ED-MD) for a system with a chiral molecule being put in the hotspot of an Ag dimer (the radii of silver spheres are 15 nm and the separation between them is 1 nm). The blue line and red line correspond to CD(ED-EQ) and CD(ED-MD), respectively. The value of CD(ED-EQ) can be as large as 9000 which is about 1000 times of the CD(ED-MD) at the wavelength of 398 nm. Besides, electric quadrupolar contribution strongly depends on the angle of molecule with respect to the surface of nanoparticles. This explains why CD signals can be dramatically influenced by the direction of molecules in experiment.

In addition to fixed number of chiral molecules, Zhang *et al*. calculated the plasmon-enhanced CD signals of large collections of oriented molecules.[87] Three systems are calculated, pure oriented chiral medium (Fig. 7(f2)), chiral medium with the symmetric distribution around the nanoribbon (Fig. 7(f3)), and chiral medium with the asymmetric distribution around the nanoribbon (Fig. 7(f4)). CD signals of these three systems are plotted in Fig. 7(f1). Similar to fixed number of chiral molecules, electric quadrupole contribution plays an primary role in the plasmon-induced CD signals for large collections oriented molecules. Furthermore, when matching the phases and their gradients for the electromagnetic fields, the CD signal can be greatly improved. As shown in Fig. 7(f1), when only one side of the nanoribbon was occupied, the CD signal (blue line) is hundreds-fold over the other two systems. Thus, for oriented molecular medium systems, matched phases are as important as the intensity of the near-field electromagnetic field.

Enhancement in plasmon-induced ROA signals has also been studied.[88,108] Figures 7(g1) and 7(g2) display maximum ROA attained by hybrid systems consisting of plasmonic nanoparticle cluster and a single molecule.[88] The enhanced ROA spectrums for dextrorotatory (*d*) and levorotatory (*l*) configurations of the nanoparticles are mirror images of each other. This maximum ROA comes from the interaction between molecular electric dipole and multiple electric dipole resonances of nanoparticle clusters.

In summary, metal nanoparticles are effective in ultrasensitive molecular chiral sensing. However, because of the resonant excitation of metallic nanoparticles, high optical losses can be induced in the plasmonic system, which would result in huge photothermal effect and property changes of the surrounding molecules.[109–111] High-permittivity nanoparticles which show extremely low optical losses, can solve this problem and have attracted particular interest in ultrasensitive detection of chiral molecules.[112–116]

4.2.1.2. Dielectric nanoparticles

In addition to the low optical losses, high refractive dielectric nanoparticles such as Si and Se nanospheres, can also achieve a spatially average enhancement of the optical chirality because of overlapping high-order electric and magnetic Mie resonances in phase, which can result in significant enhancement for the nearby molecular CD signals.[112,117] Experimentally, an enhancement of visible wavelength CD for chiral HgS nanocrystals was reported by amorphous Se nanospheres system, as shown in Fig. 8(a).[113] The system is illuminated with CPL. In contrast to the pure HgS nanocrystals, the spatially averaged CD enhancement factor was estimated to be 4.7 ± 1.5 folds for the Se nanospheres absorbed with chiral HgS nanocrystals, with the peak enhancement at particular location probably >10.

The chiroptical and temperature effect between Si and Au nanosphere were compared theoretically in Figs. 8(b1)–8(b4).[114] Figures 8(b1) and 8(b2) display the equilibrium distributions of temperature increment around Si and Au nanospheres. The radius is 65 nm for the Si/Au nanosphere, and the distance in the dimer is 5 nm. The dark/bright ones are Si/Au nanoparticle, respectively. The increased temperature around the Si (black dotted line) and Au (red dotted line) nanospheres as a function of the wavelength are plotted in Figs. 8(b3) and 8(b4). For both single nanosphere and dimer system, the temperature for Si system is much lower than Au system during the process of CD measurement. Figures 8(b3) and 8(b4) also plot enhanced CD signals based on the Si (black solid line) and Au (red solid line) nanospheres as a function of the wavelength. It is shown that CD enhancement is always stronger for Si-based nanoparticles than Au-based plasmonic counterparts because of the simultaneous electric and magnetic resonances in Si nanostructures.

Enhancement of molecular ROA signals utilizing dielectric nanoparticles has also been studied.[115,116] The ROA signal can be significantly enhanced by silicon nanoparticles due to the large magnetic field concentrated near the nanoparticle and the boosted molecular magnetic dipole emission. Electric fields symmetric breaking caused by the magnetic dipole response of Si nanoparticles is another important reason for this enhancement. The schematic of this enhancement is shown in Fig. 8(c).[115] Except for the surface-enhanced ROA (SEROA) signal, circular intensity difference (CID), which characterize the signal-to-background ratio, can also be enhanced. For single nanoparticle, the SEROA signal of Si nanoparticle can be 5 times larger than that of Au nanoparticle, with CID be improved by a factor of 10. For Si and Au nanoparticle dimers, when molecules are put in the hotspot, although SEROA signals are almost the same for these two systems, the CID of Si nanoparticle dimers can be 60 times larger than that of Au dimers.

Thus, dielectric nanoparticles can effectively enhance molecular chiral signals. However, the small area for chiral molecules to adsorb and the modest enhancement factor limit their broad application in the ultrasensitive chiral sensing. Compared to nanoparticles, metasurface structures can generate large areas with uniform enhanced optical chirality, offering more opportunities to enhance the spatial average chiroptical signal.

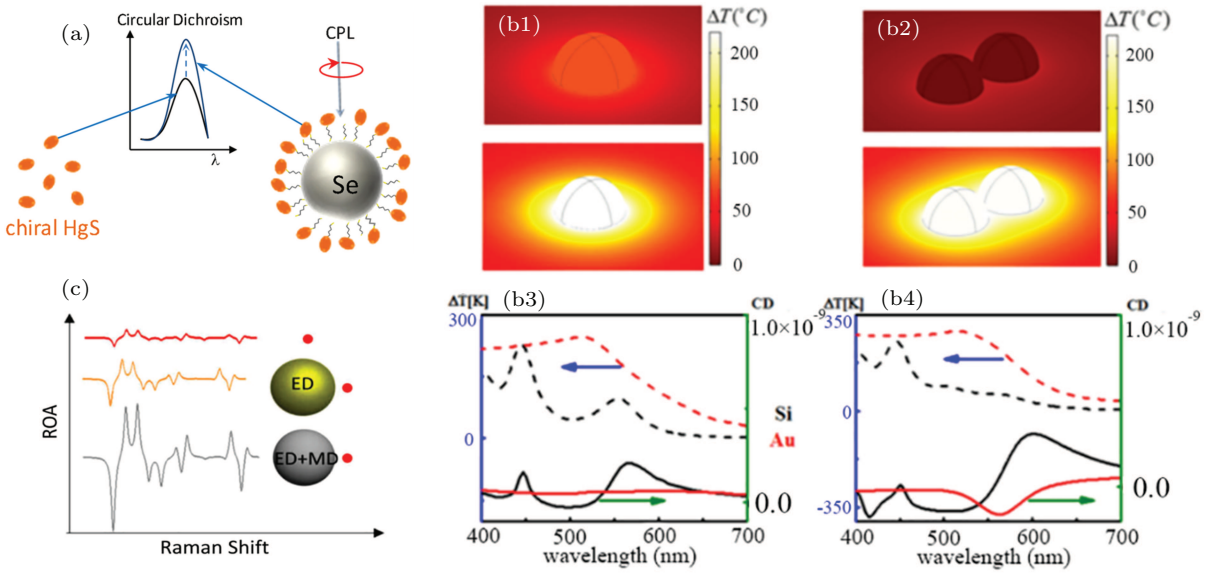


Fig. 8. (a) The schematic diagram of Se nanospheres absorbed with chiral HgS nanocrystals, and the corresponding CD spectrum of the composite and chiral HgS nanocrystal.[113] [(b1) and (b2)] Equilibrium distributions of temperature increment around the Si (upper) and Au (lower) single nanosphere (b1) and dimer (b2) systems at the wavelengths with corresponding maxima of CD signals. [(b3) and (b4)] Temperature increment (dotted lines) and CD signals (solid lines) as a function of the wavelength for the Si (black line), Au (red line) single nanosphere (b3), and dimer (b4) systems.[114] (c) Schematic diagram of pure molecular signal (red line), molecular ROA signals enhanced by metal nanoparticles (orange line) and dielectric nanoparticles (gray line).[115]

4.2.2. Planar achiral nanostructures

Figure 9(a1) displays a cavity-coupled plasmonic achiral system supporting ultrasensitive chiro-sensing.[118] This plasmonic system is comprised of arrays of gold hole-disk coupled with an asymmetric Fabry–Perot cavity, as shown in Fig. 9(a1). The coherent interaction between the localized surface plasmon and the cavity enhances the plasmonic resonance, and generates a uniform single-handed chiral near-field which flips handedness only when the handedness of incident light is reversed. The CD signals of chiral molecules adsorbed on planar gold mirror, detuned, and tuned plasmonic substrate were shown in Fig. 9(a2). As shown, about 4 orders of magnitude enhancement of vibrational chiral dichroism (VCD) signal was demonstrated via this plasmonic nanostructure.

The Purcell effect explains the enhancement of the spontaneous decay rate of achiral molecules by optical resonators. Yoo and Park extended Purcell's work to the chiral light-matter interaction in optical resonators and studied the cavity modified spontaneous decay rate of chiral molecules.[119] The authors proposed a double fishnet cavity resonator structure to demonstrate the feasibility of resonator enhanced chiroptical spectroscopy. The double fishnet structure comprises metal–dielectric–metal (MDM) multilayers, with the cavity act as a nanoscale cuvette containing chiral molecules, as shown in Fig. 9(b1). Strong CD enhancement was found locally inside the cavity without changing the sign, which is shown in Fig. 9(b2). Averaged chiroptical signal enhancement factor over the entire cavity region can be the order of tens. In addition, the resonance wavelength at which great CD signal enhancement occurs can be tuned by stacking more MDM layers or changing the cavities size according to molecular species.[13,122,124]

Mohammadi *et al.* demonstrated an analytic study on CD enhancement for chiral molecules on arbitrary nanophotonic substrate.[120] They derived closed-form expressions of the CD signal and gave guidelines for optimal nanophotonic design. Based on the analytic study, achiral periodic silicon nanodisks were proposed for the molecular CD signal enhancement. The schematic diagram of the system is shown in Fig. 9(c1). CD signals for a layer of chiral sample with 20-nm thickness placed on top of silicon nanodisks were calculated. The CD signals were in mirror image for molecules with opposite chirality. Besides, the CD signals were strongly enhanced both at the wavelength of electric dipole and magnetic dipole response as well as between the two resonances, with the enhancement factor is about 30 at the resonance and about 10–20 between the resonances, as shown in Fig. 9(c2). In addition to nanodisks, metasurface composed of periodic holey silicon disks was proposed.[125] Compared to silicon nanodisk, the holes allow direct access for chiral molecules and superchiral fields, beneficial to greater enhancement for molecular CD signals.

Experimentally, chiral molecular detection based on silicon nanocylinders was undertaken in the visible-near infrared

(VIS-NIR) region.[121] The height and diameter of nanocylinders were both optimized to ensure simultaneously exciting of the electric and magnetic resonances. 200-nm thick layers of homogeneous, randomly oriented L-, D-, and racemic mixtures of phenylalanine molecules were sequentially evaporated on silicon nanocylinders, as shown in Fig. 9(d1). The enhanced CD signals were shown in Fig. 9(d2). The red and blue curves correspond to the left- and D-enantiomer of phenylalanine deposited on Si nanocylinders. The gray lines correspond to CD signal of the bare sensor. As can be seen, compared with CD signal from bare molecules, a 300-fold optical chirality enhancement factor was obtained.

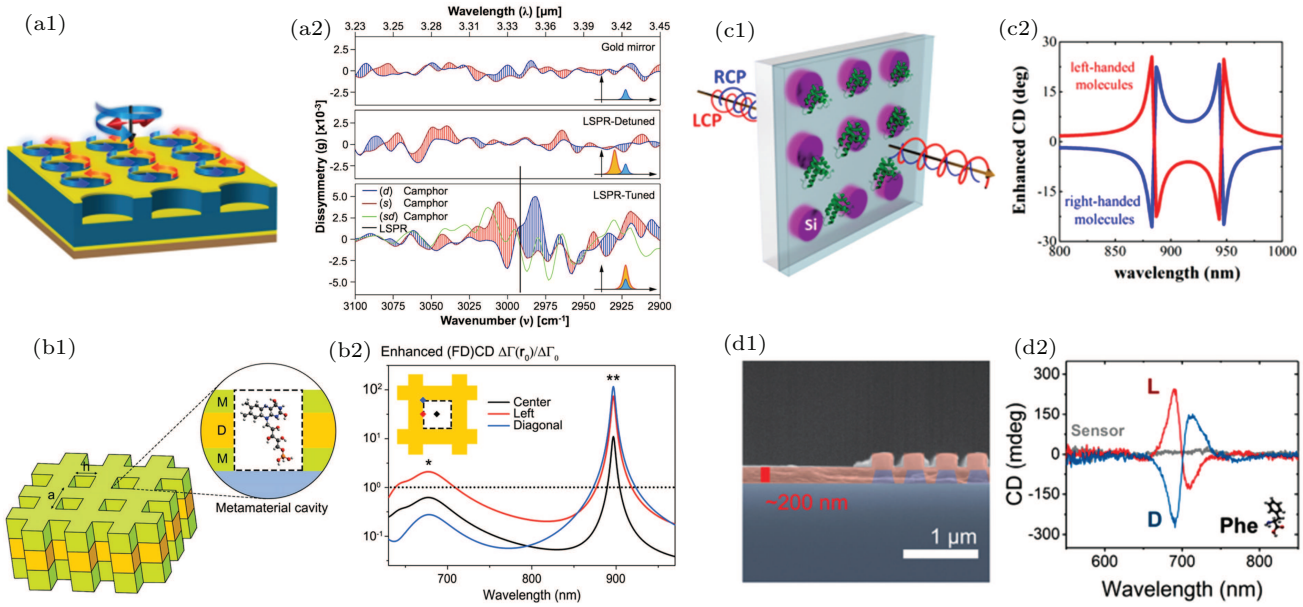


Fig. 9. (a1) Schematic diagram of cavity-coupled hole-disk array plasmonic system. (a2) Dissymmetry factors for chiral molecules on planar gold mirror, detuned, and tuned achiral plasmonic substrates (from top to bottom). Vertical line represents the LSPR of the tuned substrate.[118] (b1) The schematic diagram of double fishnet structure. Inset shows a vertical cross section of the metamaterial cavity containing molecules. (b2) The (FD) CD signal of molecules at the center (black), left (red), and upper left (blue) positions inside the cavity. Inset shows a horizontal cross section of the double fishnet structure and molecular positions.[119] (c1) Schematic diagram of chiral sample placed on top of the achiral substrate. (c2) Calculated CD signal for two chiral samples with different signs of Pasture parameter.[120] (d1) Scanning electron micrograph of the transverse section of Si sensors (purple colored) coated with a 200-nm thick phenylalanine coating (red-colored). (d2) Experimental CD spectra of the bare (grey line) and coated L- (red line) and D-enantiomers (blue line) sensors for a 120 μm×120 μm cylinder array with 130-nm height, 160-nm diameter, and 420-nm period.[121]

5. Summary and outlook

In this review, we summarized the application of chiral and achiral nanostructures in ultrasensitive chiral sensing. Both two types of structures can generate superchiral field and extremely enhance the molecular chiral signals. In general, molecular chirality detection using chiral nanostructures is based on the different resonance wavelength shifts between LH and RH nanostructures. However, chiral nanostructures have their own geometrical CD signals even without chiral molecules, thus the total CD signals have contributions both from molecules and chiral nanostructures background. It is challenge to discriminate molecular CD from total chiroptical spectrums. Achiral nanostructures are free of background chiroptical signals and can result in total CD signals only depend on the handedness of molecules. Both plasmonic and dielectric achiral nanostructures show a potential application toward ultrasensitive chiral sensing. For plasmonic nanostructures, it is challenge to generate uniform chiral near fields because of their magnetic modes are either weak or spectrally separated far from electric resonances. Specially designed plasmonic nanostructures, such as metal-insulator-metal, metallic split-ring resonators and complementary structures, can solve this problem and support both excited electric and magnetic responses at the optical frequency. However, the optical loss in plasmonic nanostructures is high because of the resonant excitation, resulting in limitation in the application of chiral detection. Dielectric nanostructures, on the other hand, show extremely low optical losses. Besides, they can generate uniform superchiral near fields because of the simultaneously excited intense magnetic and electric resonances, making dielectric nanostructures promising platforms for the ultrasensitive detection of chiral molecules.

To summarize, the field of chiral biosensing based on nanostructures is still at its early stage. A clearer understanding of the mechanism in the interaction of chiral molecules and the near chiral fields in future works will facilitate the search for more advanced nanosystems for ultrasensitive chiral sensing, and people can expect more exciting results in the near future.

References

[1] Thomson B K and Thomson W 2010 *Baltimore lectures on molecular dynamics and the wave theory of light* (Cambridge: Cambridge University Press)
[2] Valev V K, Baumberg J J, Sibilia C and Verbiest T 2013 *Adv. Mater.* **25** 2517

[3] King C and Kendrick F 1962 *The Lancet* **280** 1116
[4] Wang X O, Li C F and Li J Q 2006 *Chin. Phys. B* **15** 2623
[5] Schellman J A 1975 *Chem. Rev.* **75** 323
[6] Nafie L A 2011 *Vibrational optical activity: principles and applications* (John Wiley & Sons)
[7] Barron L D 2009 *Molecular light scattering and optical activity* (Cambridge: Cambridge University Press)
[8] Barron L D 2015 *Biomedical Spectroscopy and Imaging* **4** 223
[9] Mutter S T, Zielinski F, Popelier P L and Blanch E W 2015 *Analyst* **140** 2944
[10] Shen H X, Wu G Z and Wang P J 2013 *Acta Phys. Sin.* **62** 153301 (in Chinese)
[11] Shen H X, Wu G Z and Wang P J 2013 *Acta Phys. Sin.* **62** 053301 (in Chinese)
[12] Shen H X, Wu G Z and Wang P J 2012 *Chin. Phys. B* **21** 123301
[13] Tang Y and Cohen A E 2010 *Phys. Rev. Lett.* **104** 163901
[14] Tang Y and Cohen A E 2011 *Science* **332** 333
[15] Lipkin D 1964 *J. Math. Phys.* **5** 696
[16] Smart A G 2011 *Phys. Today* **64** 16
[17] Salam A J 2010 *Molecular quantum electrodynamics* (John Wiley & Sons)
[18] Craig D and Thirunamachandran T 1999 *Theor. Chem. Acc.* **102** 112
[19] Harris R 1965 *J. Chem. Phys.* **43** 959
[20] Ogier R, Fang Y, Svedendahl M, Johansson P and Käll M 2014 *ACS Photon.* **1** 1074
[21] Nair G, Singh H J, Paria D, Venkatapathi M and Ghosh A 2014 *J. Phys. Chem. C* **118** 4991
[22] Schäferling M, Dregely D, Hentschel M and Giessen H 2012 *Phys. Rev. X* **2** 031010
[23] Takahashi S, Potts A, Bagnall D, Zheludev N I and Zayats A V 2005 *Opt. Commun.* **255** 91
[24] Schnell M, Sarriugarte P, Neuman T, Khanikaev A, Shvets G, Aizpurua J and Hillenbrand R 2016 *Nano Lett.* **16** 663
[25] Karimullah A S, Jack C, Tullius R, Rotello V M, Cooke G, Gadegaard N, Barron L D and Kadodwala M 2015 *Adv. Mater.* **27** 5610
[26] Kuwata-Gonokami M, Saito N, Ino Y, Kauranen M, Jefimovs K, Vallius T, Turunen J and Svirko Y 2005 *Phys. Rev. Lett.* **95** 227401
[27] Konishi K, Sugimoto T, Bai B, Svirko Y and Kuwata-Gonokami M 2007 *Opt. Express* **15** 9575
[28] Bai B, Svirko Y, Turunen J and Vallius T 2007 *Phys. Rev. A* **76** 023811
[29] Schwanecke A, Krasavin A, Bagnall D, Potts A, Zayats A and Zheludev N 2003 *Phys. Rev. Lett.* **91** 247404
[30] Papakostas A, Potts A, Bagnall D, Prosvirnin S, Coles H and Zheludev N 2003 *Phys. Rev. Lett.* **90** 107404
[31] Meinzer N, Hendry E and Barnes W L 2013 *Phys. Rev. B* **88** 041407
[32] Jain P K, Eustis S and El-Sayed M A 2006 *J. Phys. Chem. B* **110** 18243
[33] Zentgraf T, Meyrath T, Seidel A, Kaiser S and Giessen H 2007 *Phys. Rev. B* **76** 033407
[34] Hendry E, Mikhaylovskiy R V, Barron L D, Kadodwala M and Davis T J 2012 *Nano Lett.* **12** 3640
[35] Esposito M, Tasco V, Cuscuna M, Todisco F, Benedetti A, Tarantini I, Giorgi M D, Sanvitto D and Passaseo A 2015 *ACS Photon.* **2** 105
[36] Gibbs J, Mark A, Eslami S and Fischer P 2013 *Appl. Phys. Lett.* **103** 213101
[37] Gibbs J G, Mark A G, Lee T C, Eslami S, Schamel D and Fischer P 2014 *Nanoscale* **6** 9457
[38] Höflich K, Yang R B, Berger A, Leuchs G and Christiansen S 2011 *Adv. Mater.* **23** 2657
[39] Esposito M, Tasco V, Cuscuna M, Todisco F, Benedetti A, Tarantini I, Giorgi M D, Sanvitto D and Passaseo A 2015 *ACS Photon.* **2** 105
[40] Esposito M, Tasco V, Todisco F, Benedetti A, Sanvitto D and Passaseo A 2014 *Adv. Opt. Mater.* **2** 154
[41] Kuzyk A, Schreiber R, Fan Z, Pardatscher G, Roller E M, Högele A, Simmel F C, Govorov A O and Liedl T 2012 *Nature* **483** 311
[42] Shen X, Song C, Wang J, Shi D, Wang Z, Liu N and Ding B 2012 *J. Am. Chem. Soc.* **134** 146
[43] Schaäferling M, Yin X, Engheta N and Giessen H 2014 *ACS Photon.* **1** 530
[44] Tseng M L, Lin Z H, Kuo H Y, Huang T T, Huang Y T, Chung T L, Chu C H, Huang J S and Tsai D P 2019 *Adv. Opt. Mater.* **7** 1900617
[45] Schaferling M, Engheta N, Giessen H and Weiss T 2016 *ACS Photon.* **3** 1076
[46] Xiong X, Sun W H, Bao Y J, Wang M, Peng R W, Sun C, Lu X, Shao J, Li Z F and Ming N B 2010 *Phys. Rev. B* **81** 075119
[47] Esposito M, Tasco V, Todisco F, Cuscunà M, Benedetti A, Sanvitto D and Passaseo A 2015 *Nat. Commun.* **6** 1
[48] Ni J, Liu S, Wu D, Lao Z, Wang Z, Huang K, Ji S, Li J, Huang Z, Xiong Q, Hu Y, Chu J and Qiu C W 2021 *Proc. Natl. Acad. Sci. USA* **118** e2020055118
[49] Kaschke J, Blume L, Wu L, Thiel M, Bade K, Yang Z and Wegener M 2015 *Adv. Opt. Mater.* **3** 1411
[50] Li J, Wang M, Wu Z, Li H, Hu G, Jiang T, Guo J, Liu Y, Yao K, Chen Z, Fang J, Fan D, Korgel B A, Alu A and Zheng Y 2021 *Nano Lett.* **21** 973
[51] Tullius R, Karimullah A S, Rodier M, Fitzpatrick B, Gadegaard N, Barron L D, Rotello V M, Cooke G, Lapthorn A and Kadodwala M 2015 *J. Am. Chem. Soc.* **137** 8380
[52] Zhao Y, Askarpour A N, Sun L, Shi J, Li X and Alù A 2017 *Nat. Commun.* **8** 1
[53] Tullius R, Platt G W, Khosravi Khorashad L, Gadegaard N, Lapthorn A J, Rotello V M, Cooke G, Barron L D, Govorov A O and Karimullah A S 2017 *ACS Nano* **11** 12049
[54] Hendry E, Carpy T, Johnston J, Popland M, Mikhaylovskiy R, Lapthorn A, Kelly S, Barron L, Gadegaard N and Kadodwala M 2010 *Nat. Nanotechnol.* **5** 783
[55] Kakkar T, Keijzer C, Rodier M, Bukharova T, Taliansky M, Love A J, Milner J J, Karimullah A S, Barron L D, Gadegaard N, Lapthorn A J and Kadodwala M S 2020 *Light Sci. Appl.* **9** 1
[56] Rodier M, Keijzer C, Milner J, Karimullah A S, Barron L D, Gadegaard N, Lapthorn A J and Kadodwala M 2019 *J. Phys. Chem. Lett.* **10** 6105
[57] Wu T, Ren J, Wang R and Zhang X 2014 *J. Phys. Chem. C* **118** 20529
[58] García-Etxarri A and Dionne J A 2013 *Phys. Rev. B* **87** 235409
[59] Zhao X and Reinhard B M 2019 *ACS Photon.* **6** 1981
[60] Alizadeh M and Reinhard B M 2015 *ACS Photon.* **2** 361
[61] Yoo S, Cho M and Park Q-H 2014 *Phys. Rev. B* **89** 161405
[62] Wu T, Zhang W, Zhang H, Hou S, Chen G, Liu R, Lu C, Li J, Wang R and Duan P 2020 *Phys. Rev. Lett.* **124** 083901
[63] García-Etxarri A, Gómez-Medina R, Froufe-Pérez L S, López C, Chantada L, Scheffold F, Aizpurua J, Nieto-Vesperinas M and Sáenz J J 2011 *Opt. Express* **19** 4815
[64] Cao H and Wiersig J 2015 *Rev. Mod. Phys.* **87** 61
[65] Tian X, Fang Y and Sun M 2015 *Sci. Rep.* **5** 17534
[66] Biagioni P, Savoini M, Huang J S, Duò L, Finazzi M and Hecht B 2009 *Phys. Rev. B* **80** 153409
[67] Yao K and Liu Y 2018 *Nanoscale* **10** 8779
[68] Reinhard B M, Siu M, Agarwal H, Alivisatos A P and Liphardt J 2005 *Nano Lett.* **5** 2246
[69] Bakker R M, Permyakov D, Yu Y F, Markovich D, Paniagua-Domínguez R, Gonzaga L, Samusev A, Kivshar Y, Luk'yanchuk B and Kuznetsov A I 2015 *Nano Lett.* **15** 2137
[70] Davis T and Hendry E 2013 *Phys. Rev. B* **87** 085405
[71] Horrer A, Zhang Y, Gérard D, Béal J, Kociak M, Plain J and Bachelot R 2019 *Nano Lett.* **20** 509
[72] Yan B, Boriskina S V and Reinhard B M 2011 *J. Phys. Chem. C* **115** 24437
[73] Gao S, Liu J and Zhang W 2016 *J. Phys. Chem. C* **120** 10500
[74] Schäferling M, Yin X and Giessen H 2012 *Opt. Express* **20** 26326
[75] Abdulrahman N A, Fan Z, Tonooka T, Kelly S M, Gadegaard N, Hendry E, Govorov A O and Kadodwala M 2012 *Nano Lett.* **12** 977
[76] Guo J, Song G, Huang Y, Liang K, Wu F, Jiao R and Yu L 2021 *ACS Photon.* **8** 901
[77] Qin J, Deng L, Kang T, Nie L, Feng H, Wang H, Yang R, Liang X, Tang T, Shen J, Li C, Wang H, Luo Y, Armelles G and Bi L 2020 *ACS Nano* **14** 2808
[78] Du K, Li P, Wang H, Gao K, Liu R B, Lu F, Zhang W and Mei T 2021 *Adv. Opt. Mater.* **9** 2001771
[79] Gorkunov M V, Antonov A A and Kivshar Y S 2020 *Phys. Rev. Lett.* **125** 093903
[80] Hu J, Lawrence M and Dionne J A 2019 *ACS Photon.* **7** 36
[81] Raziman T V, Godiksen R H, Muüller M A and Curto A G 2019 *ACS Photon.* **6** 2583
[82] Slocik J M, Govorov A O and Naik R R 2011 *Nano Lett.* **11** 701
[83] Wang R Y, Wang P, Liu Y, Zhao W, Zhai D, Hong X, Ji Y, Wu X, Wang F and Zhang D 2014 *J. Phys. Chem. C* **118** 9690

[84] Liu Y, Wang R and Zhang X 2014 *Opt. Express* **22** 4357
[85] Liu Y, Zhao W, Ji Y, Wang R Y, Wu X and Zhang X 2015 *Europhys. Lett.* **110** 17008
[86] Wu T, Zhang W, Wang R and Zhang X 2017 *Nanoscale* **9** 5110
[87] Zhang W, Wu T, Wang R and Zhang X 2017 *J. Phys. Chem. C* **121** 666
[88] Chuntonov L and Haran G 2013 *Nano Lett.* **13** 1285
[89] Lieberman I, Shemer G, Fried T, Kosower E M and Markovich G 2008 *Angew. Chem. Int. Ed.* **47** 4855
[90] Govorov A O, Fan Z, Hernandez P, Slocik J M and Naik R R 2010 *Nano Lett.* **10** 1374
[91] Lee S, Yoo S and Park Q H 2017 *ACS Photon.* **4** 2047
[92] Zhang H and Govorov A 2013 *Phys. Rev. B* **87** 075410
[93] Lu F, Tian Y, Liu M, Su D, Zhang H, Govorov A O and Gang O 2013 *Nano Lett.* **13** 3145
[94] McPeak K M, van Engers C D, Bianchi S, Rossinelli A, Poulikakos L V, Bernard L, Herrmann S, Kim D K, Burger S and Blome M 2015 *Adv. Mater.* **27** 6244
[95] ezanka P, Záruba K and Král V 2011 *Colloids Surf. Physicochem. Eng. Aspects* **374** 77
[96] di Gregorio M C, Ben Moshe A, Tirosh E, Galantini L and Markovich G 2015 *J. Phys. Chem. C* **119** 17111
[97] Kobayashi M, Tomita S, Sawada K, Shiba K, Yanagi H, Yamashita I and Uraoka Y 2012 *Opt. Express* **20** 24856
[98] Maoz B M, Chaikin Y, Tesler A B, Bar Elli O, Fan Z, Govorov A O and Markovich G 2013 *Nano Lett.* **13** 1203
[99] Besteiro L V, Zhang H, Plain J, Markovich G, Wang Z and Govorov A O 2017 *Adv. Opt. Mater.* **5** 1700069
[100] Nesterov M L, Yin X, Schaäferling M, Giessen H and Weiss T 2016 *ACS Photon.* **3** 578
[101] Govorov A O 2011 *J. Phys. Chem. C* **115** 7914
[102] Gerard V A, Gun'ko Y K, Defrancq E and Govorov A O 2011 *Chem. Commun.* **47** 7383
[103] Zhu F, Li X, Li Y, Yan M and Liu S 2015 *Anal. Chem.* **87** 357
[104] Xu L G, Xu Z, Ma W, Liu L Q, Wang L B, Kuang H and Xu C L 2013 *J. Mater. Chem. B* **1** 4478
[105] Zhu Z, Liu W, Li Z, Han B, Zhou Y, Gao Y and Tang Z 2012 *ACS Nano* **6** 2326
[106] Layani M E, Ben Moshe A, Varenik M, Regev O, Zhang H, Govorov A O and Markovich G 2013 *J. Phys. Chem. C* **117** 22240
[107] Levi-Belenkova T, Govorov A O and Markovich G 2016 *J. Phys. Chem. C* **120** 12751
[108] Abdali S and Blanch E W 2008 *Chem. Soc. Rev.* **37** 980
[109] Baffou G and Quidant R 2013 *Laser Photon. Rev.* **7** 171
[110] Ioffe Z, Shamai T, Ophir A, Noy G, Yutsis I, Kfir K, Cheshnovsky O and Selzer Y 2008 *Nat. Nanotech.* **3** 727
[111] Ward D R, Corley D A, Tour J M and Natelson D 2011 *Nat. Nanotech.* **6** 33
[112] Ho C-S, Garcia-Etxarri A, Zhao Y and Dionne J 2017 *ACS Photon.* **4** 197
[113] Vestler D, Ben-Moshe A and Markovich G 2019 *J. Phys. Chem. C* **123** 5017
[114] Zhang W, Wu T, Wang R and Zhang X 2017 *Nanoscale* **9** 5701
[115] Wu T, Zhang X, Wang R and Zhang X 2016 *J. Phys. Chem. C* **120** 14795
[116] Sheena T S, Devaraj V, Lee J M, Balaji P, Gnanasekar P, Oh J W, Akbarsha M A and Jeganathan K 2020 *Appl. Surf. Sci.* **515** 145955
[117] Cho Y, Huh J H, Park K J, Kim K, Lee J and Lee S 2017 *Opt. Express* **25** 13822
[118] Vázquez-Guardado A and Chanda D 2018 *Phys. Rev. Lett.* **120** 137601
[119] Yoo S and Park Q H 2015 *Phys. Rev. Lett.* **114** 203003
[120] Mohammadi E, Tsakmakidis K L, Askarpour A N, Dehkhoda P, Tavakoli A and Altug H 2018 *ACS Photon.* **5** 2669
[121] Garcia-Guirado J, Svedendahl M, Puigdollers J and Quidant R 2019 *Nano Lett.* **20** 585
[122] Yoo S, Cho M and Park Q-H 2014 *Phys. Rev. B* **89** 161405
[123] García-Meca C, Hurtado J, Martí J, Martínez A, Dickson W and Zayats A V 2011 *Phys. Rev. Lett.* **106** 067402
[124] García-Meca C, Ortuno R, Rodriguez-Fortuno F J, Marti J and Martínez A 2009 *Opt. Lett.* **34** 1603
[125] Mohammadi E, Tavakoli A, Dehkhoda P, Jahani Y, Tsakmakidis K L, Tittl A and Altug H 2019 *ACS Photon.* **6** 1939